

**TRANSPARENCY AND OPERATIONALITY
IMPROVEMENTS IN SCALED BILATERAL CONTROL
SYSTEM**

Godagama Vidana Arachchilage Gayan Asanka Perera

(119108U)



University of Moratuwa, Sri Lanka.
Electronic Theses & Dissertations
www.lib.mrt.ac.lk

Thesis submitted in partial fulfillment of the requirements for the degree Master
of Science of Engineering

Department of Electrical Engineering

University of Moratuwa

Sri Lanka

February 2015

DECLARATION

I declare that this is my own work and this thesis does not incorporate without acknowledgement any material previously submitted for a Degree or Diploma in any other University or institute of higher learning and to the best of my knowledge and belief it does not contain any material previously published or written by another person except where the acknowledgement is made in the text.

Also, I hereby grant to University of Moratuwa the non-exclusive right to reproduce and distribute my thesis, in whole or in part in print, electronic or other medium. I retain the right to use this content in whole or part in future works.

Signature:

Date:

Godagama Vidana Arachchilage Gayan Asanka Perera



University of Moratuwa, Sri Lanka.
Electronic Theses & Dissertations
www.lib.mrt.ac.lk

I endorse the declaration by the candidate

Dr. A.M.Harsha S.Abeykoon

ACKNOWLEDGEMENTS

This thesis is a partial requirement for the completion of Master of Science degree in University of Moratuwa. This text is a compilation of research work that has been carried out at the Control and Robotics Laboratory, Electrical Engineering Department, Faculty of Engineering, University of Moratuwa, Sri Lanka. This research was performed under the supervision of Dr. A.M.Harsha S. Abeykoon. I would like to express my gratitude for his continuous guidance and support to fulfill this task.

My sincere thanks and gratitude go to Prof. N. Wickramarachchi, Prof. Sisil Kumarawadu, Dr. Chandima D. Pathirana, Dr. W. D. Asanka S. Rodrigo and Dr. A. G. Buddhika P. Jayasekara, Electrical Engineering Department, Faculty of Engineering, University of Moratuwa. Being the members of the review panels, their valuable comments, encouragements and discussions in the progress review meetings helped me to fulfill this research task successfully.



University of Moratuwa, Sri Lanka.

Electronic Theses & Dissertations

www.lib.mrt.ac.lk

I deeply thank to the other postgraduate students: Mr. Branesh Pillai, Mr. Dinesh Chinthaka, Ms. Medhani Menikdiwela, Mr. Nishal Dayarathna, Ms. Maheshi Ruwanthika, Mr. Shanaka Abeysiriwardana and Mr. Viraj Muthugala who helped me in many ways during this postgraduate program. All members of the Department of Electrical Engineering, University of Moratuwa are also gratefully acknowledged. They constantly helped me during my research activity.

Godagama Vidana Arachchilage Gayan Asanka Perera

University of Moratuwa

February 2015

ABSTRACT

Scaled bilateral teleoperation is a very useful and highly researching concept in motion control arena. There are many researches available in the areas of bilateral teleoperation related performance optimizing. This research addresses the most important two objectives of the bilateral teleoperation: transparency and operability. The research consists of two main parts: Transparency and Operability Improvements in bilateral teleoperation and Inertia Estimation for Robust Bilateral Control.

In the first part of the research, a bilateral control system is proposed with the scaling factors derived in terms of the master and slave inertia values. Further, this concept is improved by introducing arbitrary force and position scaling factors in addition to the nominal inertias. The main objectives of bilateral teleoperation are to achieve the ideal transparency and operability conditions. In the proposed design, a condition for ideal transparency and operability is introduced for a bilateral teleoperation system which performs force and position scaling tasks. The system performance is analyzed considering the system frequency responses and root loci. This proposed system is simulated and verified the performance using the standard stability analysis tools.

In the second part of the research, a method to estimate the accurate master and slave inertias is proposed. Estimating the correct inertia values is very important to achieve the desired transparency and operability. The basic building block of the master and slave robots is the DC motor. Usually, the manufacturer given inertia value differs from its actual value due to various reasons. In this approach, a method to accurately estimate the DC motor inertia value is proposed. This method was tested on the real bilateral platform and proved the validity by measuring the force and position responses. The inertia value calculated using proposed method is applied to the bilateral controller and compared with the inertia values calculated using the conventional methods. The experimental results show the validity of the proposed method.

Keywords: bilateral teleoperation, bilateral scaling, force scaling, position scaling, bilateral transparency, bilateral operability, inertia estimation.

TABLE OF CONTENTS

DECLARATION	i
ACKNOWLEDGEMENTS	ii
ABSTRACT	iii
LIST OF FIGURES	vi
LIST OF TABLES	vi
1 INTRODUCTION	1
1.1 Background.....	1
1.2 Scaled Bilateral Teleoperation Literature Review.....	3
1.2.1 Overview.....	3
1.2.2 Bilateral scaling.....	4
1.2.3 Power scaling.....	5
1.2.4 Impedance scaling.....	7
1.2.5 Force/position scaling.....	12
1.2.6 Disturbance observer.....	12
1.2.7 Reaction Torque Observer.....	14
1.3 Originality.....	15
1.4 Content of the paper.....	16
2 TRANSPARENCY AND OPERATIONALITY IMPROVEMENTS	18
2.1 Transparency and Operability.....	18
2.2 Hybrid parameters.....	20
2.3 Design of scaled bilateral controller.....	21
2.4 The proposed architecture.....	22
2.5 Frequency analysis of hybrid parameters.....	26
2.6 Stability.....	27
2.7 Root locus analysis.....	29
2.8 Discussion.....	31
3 INERTIA ESTIMATION FOR ROBUST BILATERAL CONTROL	32
3.1 Introduction.....	32
3.2 System modeling.....	33
3.2.1 Conventional inertia estimation methods.....	35
3.2.2 Proposed change of inertia observer.....	35
3.2.3 Inverse motion acceleration test.....	38
3.3 Results and discussion.....	39
3.3.1 Selecting bilateral control for inertia verification.....	39
3.3.2 Experimental setup.....	41

3.3.3	Estimation of motor inertia experimentally.....	42
3.3.4	Validating the results with bilateral teleoperation.....	45
3.4	Conclusion.....	47
4	CONCLUSIONS.....	49
4.1	Recommendation for future developments.....	50
5	REFERENCES.....	51
6	APPENDIX.....	54



University of Moratuwa, Sri Lanka.
Electronic Theses & Dissertations
www.lib.mrt.ac.lk

LIST OF FIGURES

Figure 1: Bilateral teleoperation system.	2
Figure 2: Bilateral force and position scaling	5
Figure 3: One DOF teleoperator system with an ideal power scaling.	6
Figure 4: Two-port network representation of teleoperator system.....	7
Figure 5: Scattering-wave variable architecture for bilateral teleoperation.....	9
Figure 6: General four-channel bilateral teleoperation system block diagram.	11
Figure 7: Disturbance observer.....	13
Figure 8: Reaction torque observer.....	14
Figure 9: Flow of environmental information in a general two port bilateral model	19
Figure 10: 4-channel bilateral controller with disturbance observer	20
Figure 11: Conventional bilateral control system [44]	25
Figure 12: Proposed bilateral control system.....	25
Figure 13: Frequency response of the system.....	28
Figure 14: Phase-gain plot of transparency and operability.....	29
Figure 15: Root locus analysis.....	30
Figure 16: Change of inertia observer.	36
Figure 17: Torque responses.....	38
Figure 18: Velocity response of the inverse motion acceleration test.	38
Figure 19: Frequency response of the master or slave system.....	41
Figure 20: Bilateral test platform.....	42
Figure 21: Velocity responses.....	44
Figure 22: Torque response of CIOB test.....	45
Figure 23: Position and torque responses.	46



University of Moratuwa, Sri Lanka.
Electronic Theses & Dissertations
www.lib.mrt.ac.lk

LIST OF TABLES

Table 1: System parameters used for analysis	27
Table 2: DC motor parameters.....	42
Table 3: Inertia estimation results.....	43

Chapter 1

1 INTRODUCTION

1.1 Background

The prefix “tele” is a Greek word to denote “at a distance”. Teleoperation means operating a machine at a distance using a set of commands communicated over a communication channel. Teleoperation provides the remote sense of the distant environment and makes the operator feel the similar conditions as those at the remote location [1].

Most of the controllers that we come across in day today lives are unilateral controllers. As the name implies, communication is done unilaterally. Simple TV remote controller is an example for a unilateral controller. In a bilateral controller, master (operator) and slave (environment) sides are controlled bilaterally. The intention is to feel the environment at the distance while it is being controlled. Bilateral control system enables the slave side environment to be reflected in the master side and master side operating intention to be reflected in the slave side.

The bilateral control system is a popular and successful concept behind several engineering applications such as mine cleaning, space robots and medical surgeries. The aim of bilateral teleoperation concept is to provide a better haptic perception to the operator while performing a remote operation task. The operator should feel as if he is physically present at the remote environment (“telepresence”).

Humans have five sensors for vision, smell, sound, taste and touch. Though sound and visual sensors of the human can be stored and reproduced in a remote place, the sense of the nose (smell) and tongue (taste) cannot normally be transmitted nor stored in an electronic means. The fifth sensor, the touch can be transmitted and

reproduced using the bilateral control concept. The target of bilateral control is the transmission of haptic information by electronic means from a remote location.

In microsurgery applications, the master and slave motion spaces are dissimilar, and hence scaling factors can be applied to extend human operator's skills to small surgical areas [2]. The master manipulator's movement and the applied force can be scaled down to perform micro level operations (macro manipulation at the master and micro manipulation at the slave or vice versa according to the requirement).

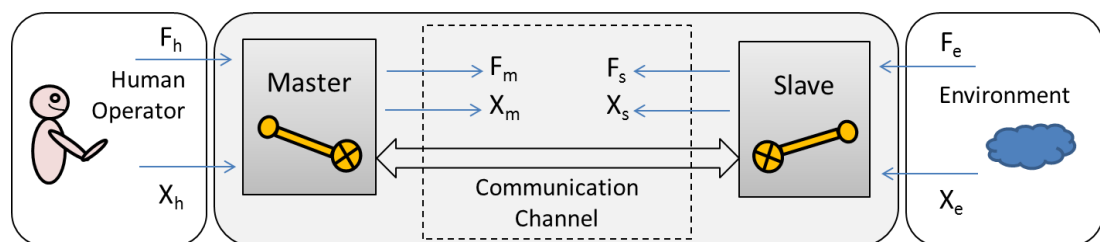


Figure 1: Bilateral teleoperation system.

The principle of bilateral teleoperation is the realization of natural law of motion of two objects (Figure 1). The human operator applies a force of F_h on the master manipulator and moves it by X_h . These force and position measurements are transmitted to the slave manipulator over a communication channel. The reaction force caused by the environment F_e and the movement of the slave manipulator X_e are fed back to the master. The master manipulator is equipped with actuators to be able to exert forces on the operator. Basically the sense of touch is made by the sensation, position and the force acting on them. This information is gathered by different sensors [3]. The communication channel always introduces a finite time delay. However, in many practical application the time delay and channel noise are assumed as negligible.

The benefits of bilateral scaling in industrial environment are manifold. It definitely leads to cost reduction by integrating with accurate robot platforms and effective

work handling. Scaling techniques are integrated in many practical applications to improve the existing drawbacks of control systems.

1.2 Scaled Bilateral Teleoperation Literature Review

1.2.1 Overview

The first successful bilateral teleoperation using master-slave manipulators was recorded in 1940s when R. Goertz and his team developed a mechanical pantograph applying the bilateral teleoperation concept. These manipulators were built to handle nuclear material of a nuclear reactor [4]. Since that invention by R. Goertz, the bilateral teleoperation techniques were developed rapidly using different scaling approaches.

Since the inception of modern bilateral teleoperation in 1940s, the operationality of the bilateral controller was developed using different scaling techniques. The applicability of bilateral scaling concept was developed from the deep sea explorations (1950s) to today's haptic related industrial applications, and since then the concept of bilateral scaling has evolved greatly and contributed to many sectors ranging from robot assisted surgery to hazardous material handling.

In 1962, Cornell Aeronautical Laboratory studied a master-slave robotic system as a man-amplifier to scale up the soldiers' lifting and carrying capabilities [5]. The same master-slave system was developed by General Electric Co from 1960 to 1971, and it was called the Hardiman [6,7]. Hardiman was a prototype man-amplifier (exoskeleton) worn by a human operator. However, man-amplifiers did not meet with much initial success because it required too much concentration of the part of the operator.

Supervisory control for teleoperation was proposed by Sheridan [8] in 1970 as a combined concept of teleoperation and automatic control. This concept was used for

teleoperation in space or in undersea operations with time scaling techniques to solve the problem of transmission time delay [9].

In 1988, Raju [10] presented the impedance scaled teleoperation techniques and suggested impedance adjustments of the teleoperation system to improve the haptic performance. The extensions of impedance scaling were proposed by Sakaki [9] and Colgate [7,11] in early 1990s. In parallel to these studies, the integration of force, position and impedance scaling techniques resulted in sophisticated teleoperation activities such as robot assisted minimally invasive surgeries and micro assembly [12,13]. As a result of these advanced teleoperation approaches, a popular telesurgery application called “Da Vinci surgical system” [14] was developed by Intuitive Surgical Inc. It is a laparoscopic assist device that enables surgeons to perform complex surgeries in a minimally invasive fashion [15].

1.2.2 Bilateral scaling

In bilateral teleoperation, normally it is expected the environment to be sensed as it is. However, sensing the environment as it is at the operator might not be practical depending on the task performed by the slave manipulator. For example, as shown in Figure 2, if the operator tries to lift a heavy object using the control force and position applied at the master manipulator, those force/position measurements should be scaled up when they are reproducing at the slave manipulator. Similarly, the feedback of force/position measurements from the environment should be scaled down when it is transmitted towards the operator to ensure the comfort of the operator.

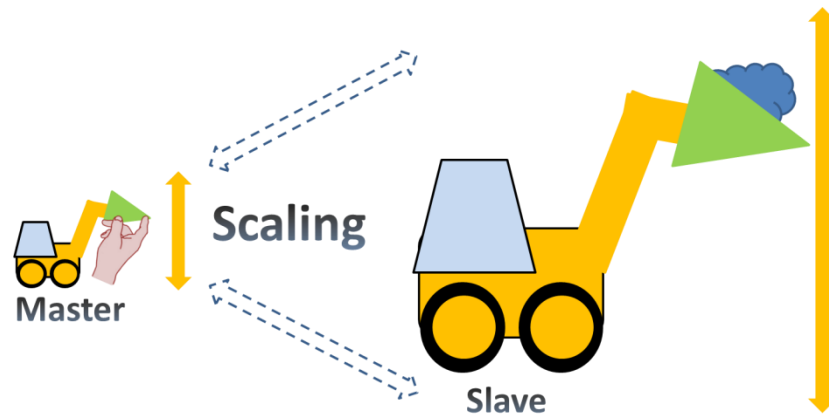


Figure 2: Bilateral force and position scaling concept with dis-similar master and slave models

Bilateral scaling mainly consists of position, force and impedance scaling methods and sometimes time scaling. Many researchers and organizations in teleoperation arena have developed the theories and models using one of position, force, impedance and time scaling methods or a hybrid of them.



University of Moratuwa, Sri Lanka.
Electronic Theses & Dissertations

www.lib.mrt.ac.lk

1.2.3 Power scaling

In 1960s, Mosher [6] used power and impedance scaling bilateral manipulators for strength increasing "man-amplifiers" called Hardiman. A similar manipulator named "extender" [16] was introduced by Kazerooni in 1980s. In his design, the operator is intimately connected to the powered limb of the extender and communicates with the extender via both power and information.

Later, in early 1990s, Colgate [7] presented a condition for robust stability in power scaled bilateral teleoperation system. Assuming passive environment, Colgate described his approach in terms of scattering matrices [17]. In this approach, the passivity is assumed when an LTI n-port network with a scattering matrix $S(j\omega)$ is satisfied the condition of $\|S(j\omega)\|_{\infty} \leq 1$.

If the scattering matrices of human operator and the environment are s_h and s_e respectively, then the corresponding scattering matrix can be represented as,

$$s_{he}(s) = \begin{pmatrix} s_h & 0 \\ 0 & s_e \end{pmatrix} \quad (1)$$

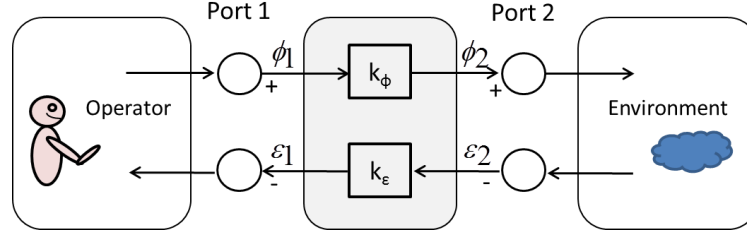


Figure 3: One DOF teleoperator system with an ideal power scaling bilateral manipulator. Where, ϕ is a flow variable and ε is an effort variable. k_ϕ and k_ε are dimensionless static scaling factors [18].

The scattering matrix for the master slave teleoperation system (Figure 3) is given by (2), where, subscripts 1 and 2 denote port 1 and port 2, and m and s stand for master and slave of the teleoperation system respectively.

$$s_{ms}(s) = \begin{pmatrix} s_{11} & s_{12} \\ s_{21} & s_{22} \end{pmatrix} \quad (2)$$

The scattering matrix of the two-port teleoperation system, is given in terms of the hybrid matrix $H(s)$ (discussed in impedance scaling section in (9)) by simple loop transformation.

$$s(s) = \begin{pmatrix} 1 & 0 \\ 0 & -1 \end{pmatrix} (H(s) - 1)(H(s) + 1)^{-1} \quad (3)$$

Again, in 1993, in a conceptually similar approach, Colgate presented the bilateral power scaling using effort and flow variables [18]. This approach can be modeled as an ideal bilateral manipulator is assumed (Figure 3) connecting a 1-port operator and 1-port environment. This system is viewed as an effort-flow pair being exchanged at each port (in the case of mechanical systems it is the force-velocity pair).

The power transferred from the operator to the master manipulator and from the environment to the slave manipulator is defined by the bilateral control law. If the effort variables (currents, velocities) are scaled with respect to each other, then it is

necessary that the flow variables (voltages, forces) to be at the inverse scale to satisfy power balancing equation.

$$\phi_1 \varepsilon_1 = -\frac{k_\varepsilon}{k_\phi} \phi_2 \varepsilon_2 \quad (4)$$

The ratio k_ε / k_ϕ is defined as the “power scaling factor”.

1.2.4 Impedance scaling

1.2.4.1 Scaling with two-port architecture

Further to the power scaling approach discussed in previous section, Colgate introduced impedance shaping bilateral control system in [18,19]. In this design, the master/slave impedances were dynamically reshaped to create an appropriate dynamic behavior of the system.

The impedance scaling factor $k_\varepsilon k_\phi$ of Figure 3 can be derived from the relationship between the impedance felt by the operator and the impedance of the environment.

$$Z_o(\phi) = k_\varepsilon k_\phi Z_e(\phi) \quad (5)$$

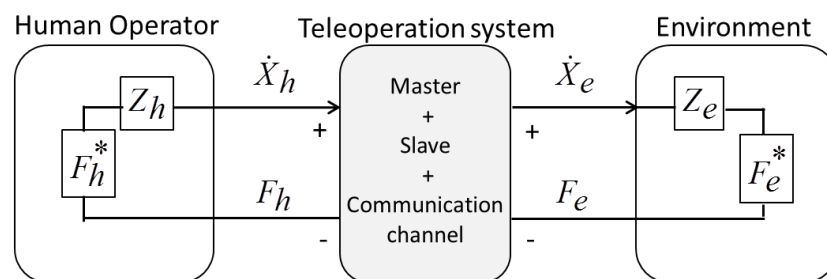


Figure 4: Two-port network representation of teleoperator system. Where, Z_h , \dot{X}_h , F_h and F_h^* , and Z_e , \dot{X}_e , F_e and, F_e^* represent impedance, velocity, force and the exogenous force input generated by the operator and the environment, respectively.

The impedance scaling approach can be modeled assuming an LTI two port teleoperation network. Similar studies are available in [10, 20-22]. Considering the

two-port network arrangement in Figure 4, following mechanical equations can be derived.

Let the effort variable be the position x and flow variable be the force F of the mechanical system model. Then, the operator and the environment impedances becomes $Z_h(s)$ and $Z_e(s)$ respectively.

$$Z_h(s) = \frac{F_h(s)}{-\dot{X}_h(s)}, \quad Z_e(s) = \frac{F_e(s)}{\dot{X}_e(s)} \quad (6)$$

The impedance matrix $Z(s)$ and admittance matrix $Y(s)$ can be obtained as follows [10].

$$\begin{pmatrix} F_h(s) \\ F_e(s) \end{pmatrix} = \underbrace{\begin{pmatrix} z_{11}(s) & z_{12}(s) \\ z_{21}(s) & z_{22}(s) \end{pmatrix}}_{Z(s)} \begin{pmatrix} \dot{X}_h(s) \\ -\dot{X}_e(s) \end{pmatrix} \quad (7)$$

$$\begin{pmatrix} \dot{X}_h(s) \\ -\dot{X}_e(s) \end{pmatrix} = \underbrace{\begin{pmatrix} y_{11}(s) & y_{12}(s) \\ y_{21}(s) & y_{22}(s) \end{pmatrix}}_{Y(s)} \begin{pmatrix} F_h(s) \\ F_e(s) \end{pmatrix} \quad (8)$$

Above system model can be represented by its hybrid matrix $H(s)$ [22], given that the force response is sensed at the slave manipulator.

$$\begin{pmatrix} F_h(s) \\ -\dot{X}_e(s) \end{pmatrix} = \underbrace{\begin{pmatrix} h_{11}(s) & h_{12}(s) \\ h_{21}(s) & h_{22}(s) \end{pmatrix}}_{H(s)} \begin{pmatrix} \dot{X}_h(s) \\ \dot{F}_e(s) \end{pmatrix} \quad (9)$$

The elements of hybrid matrix $H(s)$ can be reduced to a set of scaling facets. This interpretation has become the basis for several theoretical contributions such as the scattering approach and 4-channel model, especially to address the communication delays of the channel.

$$H(s) = \begin{pmatrix} \text{Input Impedance} & \text{Force Scale} \\ -\text{Velocity Scale} & \text{Output Admittance} \end{pmatrix} \quad (10)$$

1.2.4.2 Scaling with wave-variable architecture

Wave variable approach described in [23,24,25,26] is a similar approach to the scattering matrix based method. This concept is developed in the analysis and design of teleoperation systems with time delays. As shown in Figure 5, instead of

exchanging master-slave force and velocity signals, wave variables (a_1, a_2, b_1 and b_2) are transmitted. \dot{X}_m and F_m , and \dot{X}_s and F_s , represent velocity and force variables of master and slave manipulators, respectively. T_1 and T_2 are the time delays.

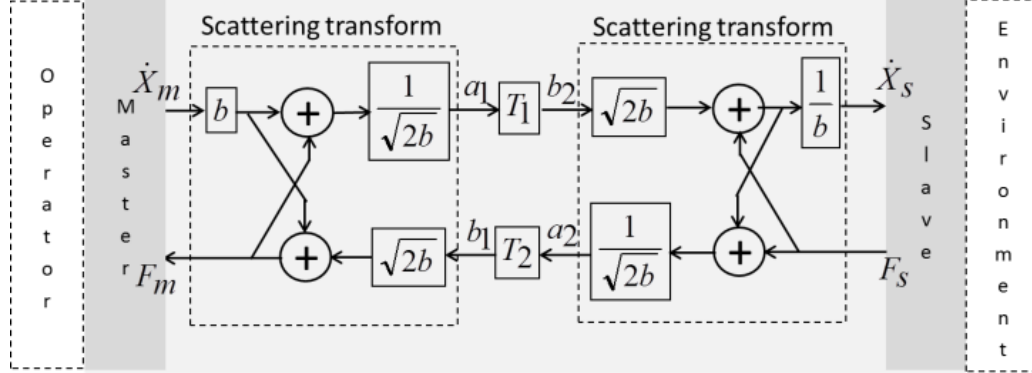


Figure 5: Scattering-wave variable architecture for bilateral teleoperation.

Wave variable method can be implemented to stabilize a system. This is accomplished by using wave transformation on both the master and slave sides. Wave variables can be expressed as inwave or incident wave $\vec{w}(s)$ and outwave or reflected wave $\vec{w}(s)$. The travelling waves are defined using an algebraic transformation expressed as follows,

$$a_1 = \frac{F_m + b\dot{X}_m}{\sqrt{2b}}, \quad a_2 = \frac{F_e + b\dot{X}_e}{\sqrt{2b}} \quad (11)$$

$$b_1 = \frac{F_m - b\dot{X}_m}{\sqrt{2b}}, \quad b_2 = \frac{F_e - b\dot{X}_e}{\sqrt{2b}} \quad (12)$$

where, b is the characteristic impedance of the transmission line which serves as a tuning parameter to tradeoff between speed of motion and level of forces. The relationship between incident wave and reflected wave is given by,

$$\vec{w}(s) = \begin{pmatrix} b_1 \\ b_2 \end{pmatrix} = \underbrace{\begin{pmatrix} S_{11} & S_{12} \\ S_{21} & S_{22} \end{pmatrix}}_{S(s)} \begin{pmatrix} a_1 \\ a_2 \end{pmatrix} = S(s)\vec{w}(s) \quad (13)$$

Several control strategies are introduced in the wave domain due to the intrinsic passivity of the wave formulation. These strategies are useful to maintain the passivity when performed directly in the power variables domain. Different types of

representations of a network can be transformed to each other, as long as the matrices are not ill-conditioned [27].

1.2.4.3 Transparency in impedance scaling

In order to perform different force/position (velocity) scaling tasks, the bilateral teleoperation system has to be transparent. When the transparency is high, the system represents the environmental impedance with high accuracy at the master side. The transparency can be achieved when the operator impedance $Z_h(s)$ and the environment impedance $Z_e(s)$ are equal.

$$Z_h(s) = Z_e(s) \quad (14)$$

When this condition is satisfied, the accurate environment impedance is transferred to the operator. This yields the hybrid matrix and scattering matrix to become,

$$H(s) = \begin{pmatrix} 0 & -1 \\ 1 & 0 \end{pmatrix}, \quad S(s) = \begin{pmatrix} 0 & 1 \\ 1 & 0 \end{pmatrix} \quad (15)$$

Susa et al. [28] following a similar hybrid matrix based approach showed that the scaling factors and controller gains can be incorporated to achieve ideal reproducibility and operability in a micro-macro bilateral system. Ideal reproducibility and operability of the micro-macro teleoperation system is achieved by the proposed impedance scaling based hybrid matrix, according to,

$$\begin{pmatrix} h_{11}(s) & h_{12}(s) \\ h_{21}(s) & h_{22}(s) \end{pmatrix} = \begin{pmatrix} \frac{M_{nm}^2}{C_f} s^2 & \beta \frac{M_{nm}}{M_{ns}} \\ \alpha \frac{M_{nm}}{M_{ns}} & 0 \end{pmatrix} \quad (16)$$

Where, master and slave nominal masses are approximated by M_{nm} and M_{ns} respectively, α and β denote position and force scaling ratios of the system respectively, and C_f represents force control gain.

1.2.4.4 Scaling with four-channel Lawrence architecture

In 1995, Salcudean [29] suggested a four channel data transmission structure to achieve the transparency of bilateral teleoperation system under position and rate

control. The four channel general teleoperator architecture (Figure 6) introduced by Lawrence [30,31] is adopted here for the proposed design. Compared to two-port model, the four port architecture is used to analyze and quantitatively compare various teleoperation schemes in terms of transparency performance and stability. This systematic approach reveals that all four information channels between master and slave are necessary to achieve good transparency.

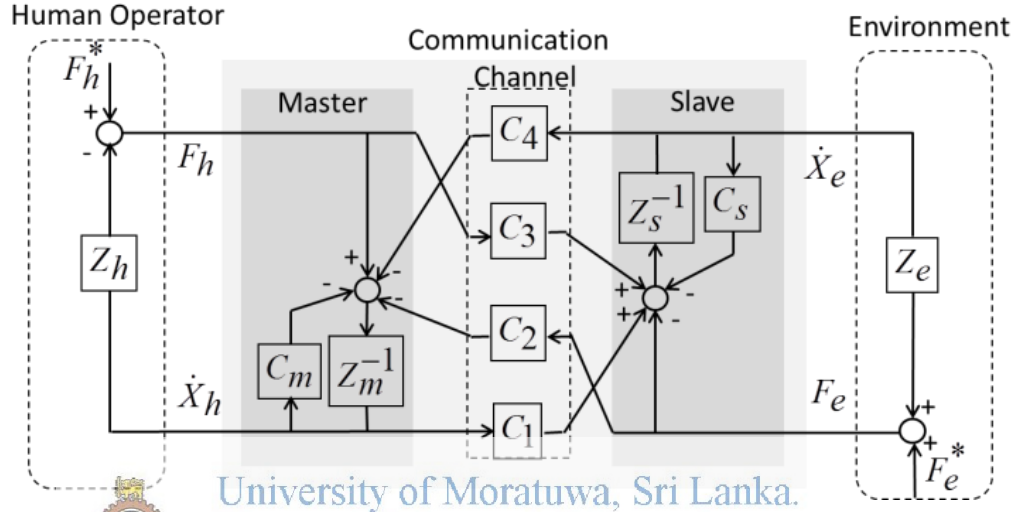


Figure 6: General four-channel bilateral teleoperation system block diagram. C_m and C_s are the transfer functions of the local controllers, and $C_1 - C_4$ are remote compensators.

As for the proposed design, the transmitted impedance felt by the operator, z_t can be expressed using the block transfer function as below [31].

$$Z_t = \frac{[(Z_m + C_m)(Z_s + C_s) + C_1 C_4] + Z_e(Z_m + C_m + C_1 C_2)}{(Z_s + C_s - C_3 C_4) + Z_e(1 - C_2 C_3)} \quad (17)$$

For a fully transparent teleoperator system, $z_t = z_e$ equation should be satisfied for any z_e . Based on these grounds, a mixed position/rate model was introduced in [29]. In this approach, the scaling between the master and slave velocity and force was realized by the hybrid matrix $H(s)$, according to,

$$H(s) = \begin{pmatrix} Z_m(s) & G(s) \\ -\frac{1}{G(s)} & 0 \end{pmatrix} \quad (18)$$

Where, $Z_m(s)$ is the master impedance and $G(s)$ is a stable transfer function. The four-channel architecture proposed by Lawrence was used in different bilateral scaling

designs and teleoperation theories. Few of the most important improvements suggested for four-channel bilateral teleoperator systems can be found in [32-35].

1.2.5 Force/position scaling

When the master and the slave manipulators operate on macro-micro architecture or vice versa, thus it is vital to select matching scaling factors to achieve the desired performance. The steady state condition of the bilateral controller can be governed by, $X_m = \alpha X_s$ and $F_m = \beta F_s$. Here, α and β are the position and force scaling factors respectively. F_m and X_m , and F_s and X_s represent force and position quantities of the master and slave manipulators, respectively.

Force and position scaling can perform transformations from the motor space to the modal space through the scaling gain matrix approach. However, in real time, actual manipulation scenarios, the scaling gain in the control should be changed arbitrary by operators for more precise operations. Kosugi et al. in [36], suggested a variable scaling gain concept to change the scaling gain arbitrary to achieve this condition. Conceptually similar force and position scaled problems are addressed in [37-40].

1.2.6 Disturbance observer

In bilateral control systems, when the disturbance torque is present, the motor does not provide the desired output. To guarantee the expected functionalities of the motor, it is important to compensate the disturbance torque. Disturbance Observer can be used here to measure the disturbance torque and compensate it to the system [55,56].

Real world systems are usually affected by external disturbances [38]. It is important to suppress these disturbances to achieve the robustness of the system. Disturbance Observer is an effective tool which can be used for this purpose. Figure 7 shows the block diagram of Disturbance Observer [42,43].

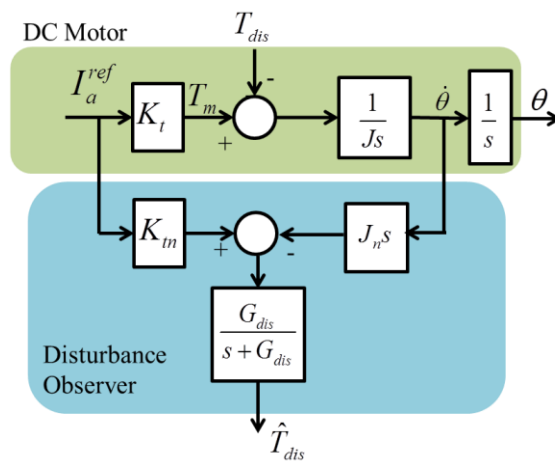


Figure 7: Disturbance observer

The inertia of the DC motor J can be changed due to the mechanical configuration of the motion system. The torque coefficient K_t also varies according to the rotor position of the electric motor due to irregular distribution of magnetic flux on the surface of rotor [41].

If the nominal motor inertia J_n varies by ΔJ and nominal torque coefficient K_m varies by ΔK_t , the actual J and K_t can be represented by (19) and (20) respectively.

$$J = J_n + \Delta J \tag{19}$$

$$K_t = K_{tn} + \Delta K_t \tag{20}$$

$$T_{dis} = K_{tm} I_a - J_n \ddot{\theta} \tag{21}$$

Disturbance torque T_{dis} consists of load torque T_l , frictional torques (coulomb friction T_f and viscous friction $B\dot{\theta}$) and torques arising from the parameter variations. I_a is the armature current.

$$T_{dis} = T_l + T_f + B\dot{\theta} + \Delta J \ddot{\theta} - \Delta K_t I_a \tag{22}$$

T_{dis} can be calculated from the right hand side known parameters of (22). Here, $\Delta J \ddot{\theta}$ and $\Delta K_t I_a$ represent the torques due to the differences in inertia and motor torque constant. \hat{T}_{dis} is the estimated disturbance torque which is the output of the disturbance observer in Figure 7 and G_{dis} is the cut-off frequency of the observer.

1.2.7 Reaction Torque Observer

Disturbance observer can be used not only for the disturbance compensation but also for reaction torque estimation. The disturbance observer is able to estimate the reaction torque without using a torque sensor by identifying the internal disturbance of the system [42].

When the motor is running with a load, the load torque exerted on the motor due to the load can be obtained from (23). As shown in Figure 8, all the disturbance components are removed at the reaction torque observer and, hence, the Reaction Torque Observer (RTOB) output is the estimated load torque \hat{T}_l by rearranging (22).

$$T_l = T_{dis} - (T_f + B\dot{\theta} + \Delta J\ddot{\theta} - \Delta K_t I_a) \quad (23)$$

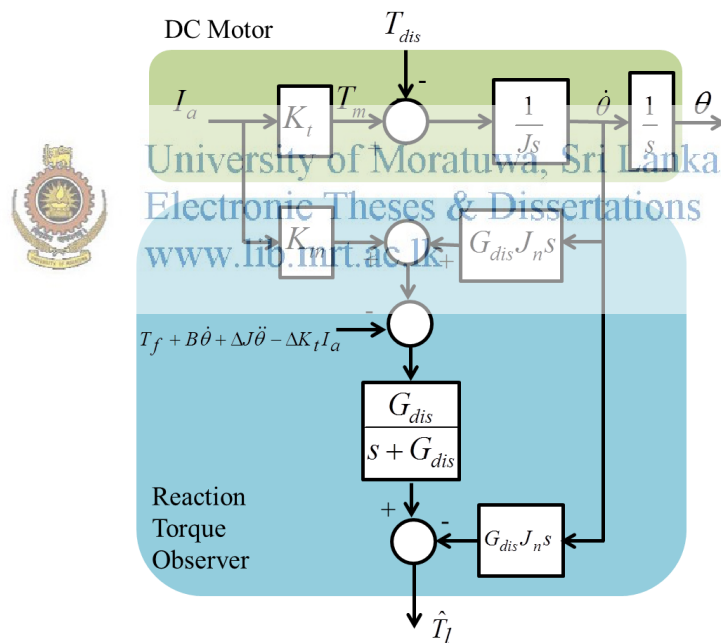


Figure 8: Reaction torque observer.

1.3 Originality

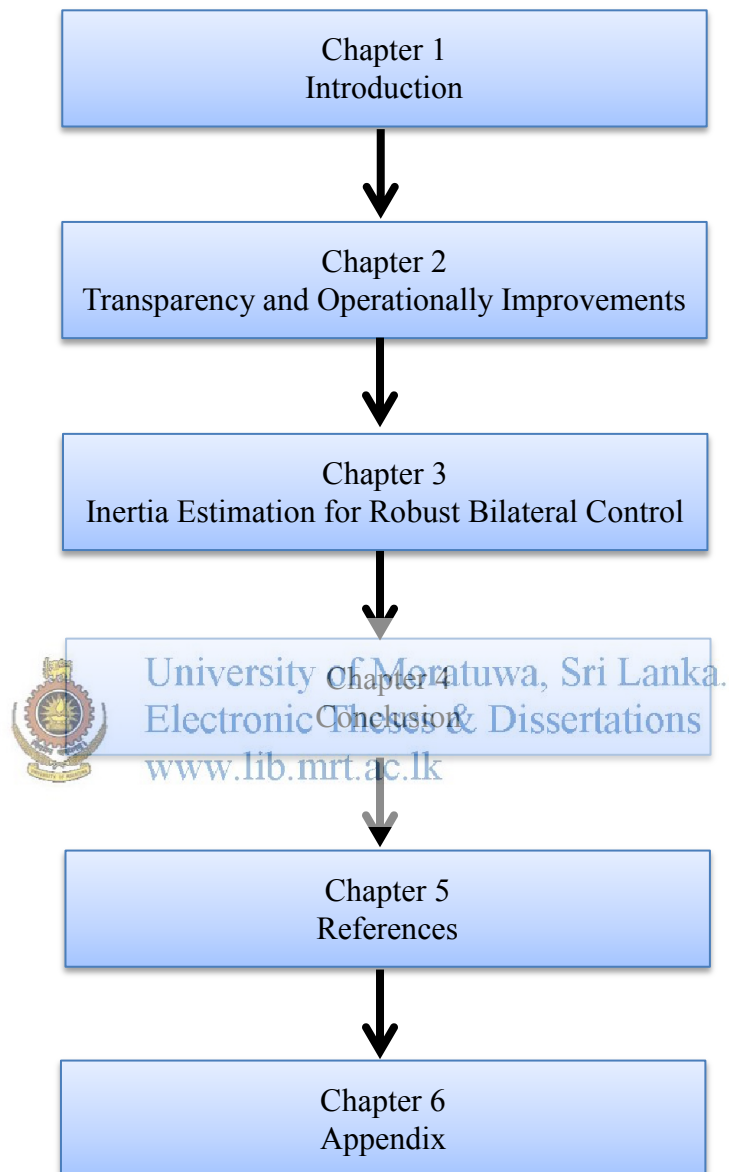
Scaled bilateral teleoperation is a very useful and highly researching concept in motion control arena. There are many research available in the areas of bilateral teleoperation related performance optimizing. This research addresses the most important two objectives of the bilateral teleoperation: transparency and operability. The research is twofold.

In the first part, a bilateral control system is proposed with the scaling factors derived in terms of the master and slave inertias. Further, this concept is improved by introducing arbitrary force and position scaling factors in addition to the nominal masses. A condition for ideal transparency and operability of scaled bilateral teleoperation is derived as the main finding of the first part. In ideal conditions, the environment impedance is represented at master side as it is, and the additional force felt by the operator in addition to the environmental reaction force is zero (14). The system performance is analyzed considering the system frequency responses and root loci. This proposed system is simulated, and verified the performance using the standard stability analysis tools.

In the second part of the research, a method to estimate the accurate master and slave inertias is proposed. Estimating the correct inertia values is very important to achieve the desired transparency and operability. This method was tested on the real bilateral platform and proved the validity.

1.4 Content of the paper

The structure of the thesis is as follows:



A summary of each chapter is mentioned below according to the chapter order.

Chapter 1

This chapter describes the background of the thesis, overview of the bilateral scaling, important theories extracted from the literature survey, research contribution and the structure of the thesis.

Chapter 2

In this chapter, the related theories for bilateral teleoperation, the system modeling for scaled bilateral teleoperation, transparency and operability improvements and stability analysis are discussed.

Chapter 3

An inertia estimation method for the DC motors of the master and slave robots is proposed in this chapter. The estimated inertia is compared with the conventional methods. Further, simulation and experimental results and analysis also included here.



University of Moratuwa, Sri Lanka
Electronic Theses & Dissertations
www.lib.mrt.ac.lk

Chapter 4

Conclusions and recommendation for future developments are presented in this final chapter.

Chapter 2

2 TRANSPARENCY AND OPERATIONALITY IMPROVEMENTS

2.1 Transparency and Operationality

The main objectives of bilateral teleoperation are to achieve the ideal transparency and operationality. Transparency is the ideal reproduction of the environment impedance at the master side. Operationality defines the additional force felt by the operator in addition to the actual environment reaction force.

Transparency is necessary for the operator to feel the environment as it is, and operationality is required for comfortable operation. In addition to these two motives, the system must be stable. When the system is unstable, the equipment damage or operator injury can happen. Therefore, it is vital the bilateral teleoperation to satisfy transparency, operationality and stability.

In bilateral teleoperation system, the master and slave are coupled with the transmission of force and position information. In ideal situations, the operator feels as if he is interacting with the environment or completely transparent.

In bilateral teleoperation, the slave side force F_s and position X_s are related by the environment impedance.

$$F_s = Z_e X_s \quad (24)$$

Where, Z_e is the environmental impedance. To achieve the ideal conditions, the master side force F_m and position should have the same relationship. If the impedance felt by the operator is Z_t , the master side relationship becomes,

$$F_m = Z_t X_m \quad (25)$$

For the same forces ($F_m = F_s$) and positions ($X_m = X_s$), the following impedance condition should be satisfied.

$$Z_t = Z_e \quad (26)$$

However, in practical applications, the ideal transparency is not achievable.

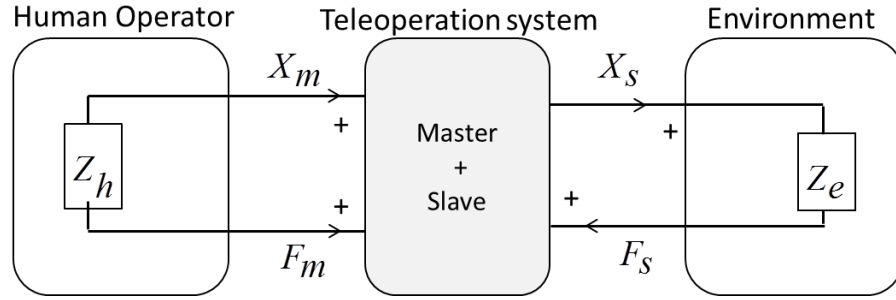


Figure 9: Flow of environmental information in a general two port bilateral model

Figure 9 shows the bilateral system model considering the opposite directions of master and slave forces. Environment in bilateral teleoperation means the operator and remote object. Environmental information is communicated as position and force of master-slave. The relationship between master and slave can be formulated by independent variables H (hybrid matrix).

$$\begin{pmatrix} F_m \\ X_m \end{pmatrix} = \begin{pmatrix} H_{11} & H_{12} \\ H_{21} & H_{22} \end{pmatrix} \begin{pmatrix} X_s \\ -F_s \end{pmatrix} \quad (27)$$


www.lib.mrt.ac.lk

The ideal hybrid matrix representation is given in (29).

$$\begin{pmatrix} H_{11} & H_{12} \\ H_{21} & H_{22} \end{pmatrix} = \begin{pmatrix} 0 & 1 \\ 1 & 0 \end{pmatrix} \quad (29)$$

The relationship between position and force in master side is given by

$$F_m = \frac{(H_{11} + H_{12}Z_e)}{(H_{21} + H_{22}Z_e)} X_m = Z_t X_m \quad (30)$$

When the environment impedance Z_e is equal to the impedance felt by the operator Z_t , the operator can feel the environment as it is.

$$F_m = \left(\frac{H_{12}Z_e}{H_{21} + H_{22}Z_e} + \frac{H_{11}}{H_{21} + H_{22}Z_e} \right) X_m \quad (31)$$

$$F_m = (P_r Z_e + P_o) X_m \quad (32)$$

Here, P_r and P_o represent transparency and operability. P_r and P_o are the functions of the environment impedance ($P_r = f_1(Z_e), P_o = f_2(Z_e)$). In bilateral control without scaling factors, the ideal transparency and operability is given as follows.

$$P_r = 1 \tag{33}$$

$$P_o = 0 \tag{34}$$

Satisfying (33) and (34) will represent the ideal environment impedance at the master side.

2.2 Hybrid parameters

The four channel general teleoperator architecture (Figure 6) was introduced by D.A. Lawrence [30,31]. It considers only the ideal condition and does not deal with friction or modeling errors. Taking this problem in to consideration, 4 channel controller with disturbance observer is represented in Figure 10 [43]. Here, C and P represent controller gain and high frequency disturbance, respectively.

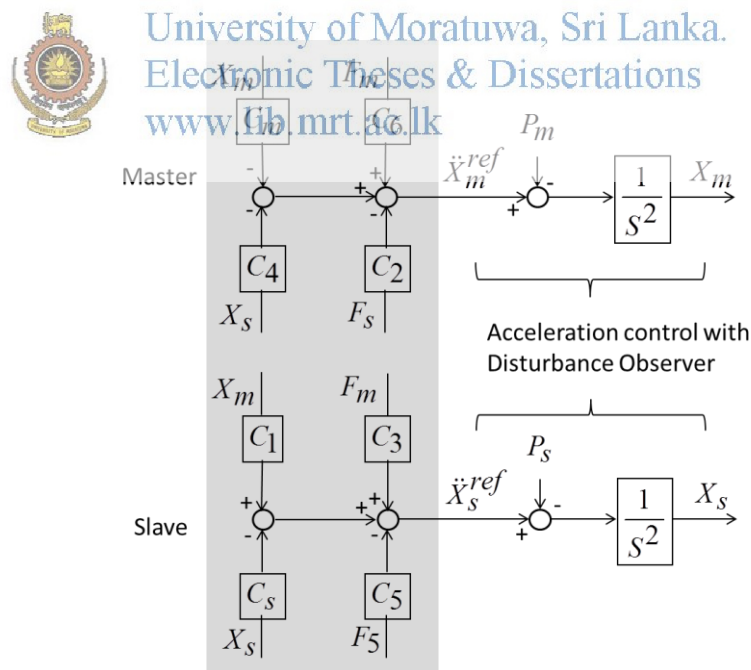


Figure 10: 4-channel bilateral controller with disturbance observer

Hybrid parameters for general 4-channel bilateral control system are given as follows [43].

$$H_{11} = \frac{C_1 C_4 + (s^2 + C_m)(s^2 + C_s)}{C_1 C_6 + C_3(s^2 + C_m)} \quad (35)$$

$$H_{12} = -\frac{C_1 C_2 + C_5(s^2 + C_m)}{C_1 C_6 + C_3(s^2 + C_m)} \quad (36)$$

$$H_{21} = \frac{-C_3 C_4 + C_6(s^2 + C_s)}{C_1 C_6 + C_3(s^2 + C_m)} \quad (37)$$

$$H_{22} = \frac{C_2 C_3 - C_5 C_6}{C_1 C_6 + C_3(s^2 + C_m)} \quad (38)$$

2.3 Design of scaled bilateral controller

In this approach, force and position scaling of bilateral teleoperation were considered. The scaling was achieved in terms of the nominal masses of master and slave and arbitrary set scaling gains. Nominal masses of the master and slave are considered for bilateral controllers with linear motors. For DC motor based systems, the motor inertia has to be considered. However, for the simplicity, in this design a bilateral control system with linear motors is assumed.



University of Moratuwa, Sri Lanka.
Electronic Theses & Dissertations
www.lib.mrt.ac.lk

Force and position relationship between master and slave can be normalized with their nominal masses.

$$X_m = \frac{M_{nm}}{M_{ns}} X_s \quad (39)$$

$$F_m = -\frac{M_{nm}}{M_{ns}} F_s \quad (40)$$

Above normalization represents the size of the systems. The operator should be able to decide the scaling ratio between master-slave parameters. Therefore, introducing position scaling factor α and force scaling factor β to (39) and (40) respectively, provides following relationships.

$$X_m = \alpha \frac{M_{nm}}{M_{ns}} X_s \quad (41)$$

$$F_m = -\beta \frac{M_{nm}}{M_{ns}} F_s \quad (42)$$

Above (41) and (42) can be further modified as follows:

$$\frac{1}{M_{nm}} X_m - \frac{1}{M_{ns}} \alpha X_s = 0 \quad (43)$$

$$\frac{1}{M_{nm}} F_m + \frac{1}{M_{ns}} \beta X_s = 0 \quad (44)$$

Representing above equation in hybrid matrix format,

$$\begin{pmatrix} F_m \\ X_m \end{pmatrix} = \begin{pmatrix} 0 & \beta \frac{M_{nm}}{M_{ns}} \\ \alpha \frac{M_{nm}}{M_{ns}} & 0 \end{pmatrix} \begin{pmatrix} X_s \\ -F_s \end{pmatrix} \quad (45)$$

The hybrid parameters of (45) are the ideal values for a bilateral control system with different masses and scaling gains. The transparency and operability conditions of this system can be derived as (46) and (47).

$$P_r = \frac{\beta}{\alpha} \quad (46)$$

$$P_o = 0 \quad (47)$$

2.4 The proposed architecture

Achieving the ideal transparency is the most important task in bilateral teleoperation. The condition for ideal transparency is derived considering the hybrid matrix approach.

$$\begin{pmatrix} H_{11} & H_{12} \\ H_{21} & H_{22} \end{pmatrix} = \begin{pmatrix} * & \beta \frac{M_{nm}}{M_{ns}} \\ \alpha \frac{M_{nm}}{M_{ns}} & 0 \end{pmatrix} \quad (48)$$

In (48), * represents an arbitrary value. The control gains are selected as follows to satisfy (48).

$$-\frac{1}{\alpha\beta} M_{ns}^2 C_4 = \frac{1}{\beta} M_{nm} M_{ns} C_m = C_p(s) \quad (49)$$

$$M_{nm}^2 C_1 = \frac{1}{\alpha} M_{nm} M_{ns} C_s = C_p(s) \quad (50)$$

$$-\frac{1}{\alpha\beta} M_{ns}^2 C_2 = \frac{1}{\alpha} M_{nm} M_{ns} C_6 = C_f(s) \quad (51)$$

$$M_{nm}^2 C_3 = -\frac{1}{\beta} M_{nm} M_{ns} C_5 = C_f(s) \quad (52)$$

Where, $C_p(s)$ and $C_f(s)$ are position control gain and force control gain, respectively. By substituting these control gains for from (35) to (38), the hybrid parameters are obtained as (53).


$$\begin{pmatrix} H_{11} & H_{12} \\ H_{21} & H_{22} \end{pmatrix} = \begin{pmatrix} \frac{M_{nm}^2}{C_f} s^2 & \beta \frac{M_{nm}}{M_{ns}} \\ \alpha \frac{M_{nm}}{M_{ns}} & 0 \end{pmatrix} \quad (53)$$

By using these hybrid parameters, P_r and P_o can be found from (31).

$$P_r = \frac{\beta}{\alpha} \quad (54)$$

$$P_o = \frac{M_{nm}M_{ns}}{\alpha C_f} s^2 \quad (55)$$

Here, (54) provides the same transparency value given by (46), and hence the transparency becomes ideal. However, (55) is not equal to (47). Therefore, the ideal operationality is not achieved. The operational force becomes small by increasing the force control gain C_f .

 **University of Moratuwa, Sri Lanka.**
Modifying above approach to achieve ideal operationality:
 The above approach can be further extended targeting ideal operationality. According to (31), H_{11} should be zero to achieve the ideal operationality.

$$\begin{pmatrix} H_{11} & H_{12} \\ H_{21} & H_{22} \end{pmatrix} = \begin{pmatrix} 0 & \beta \frac{M_{nm}}{M_{ns}} \\ \alpha \frac{M_{nm}}{M_{ns}} & * \end{pmatrix} \quad (56)$$

Here, * is an arbitrary value. Selecting control gains as follows to satisfy (56) yields:

$$C_1 = -(s^2 + C_m) \quad (57)$$

$$C_2 = -C_5 = (s^2 + C_s) \quad (58)$$

$$C_3 = -C_6 = \frac{M_{ns}}{\beta M_{nm}} (s^2 + C_s) \quad (59)$$

$$C_4 = -\left[\frac{2\alpha M_{nm}}{M_{ns}} + 1\right]s^2 + \left[C_s - \frac{2\alpha M_{nm}}{M_{ns}} C_m\right] \quad (60)$$

Applying above control gains for from (35) to (38), the hybrid parameters become,

$$\begin{pmatrix} H_{11} & H_{12} \\ H_{21} & H_{22} \end{pmatrix} = \begin{pmatrix} 0 & \beta \frac{M_{nm}}{M_{ns}} \\ \alpha \frac{M_{nm}}{M_{ns}} & 0 \end{pmatrix} \quad (61)$$

By using these hybrid parameters, P_r and P_o can be found from (31).

$$P_r = \frac{\beta}{\alpha} \quad (62)$$

$$P_o = 0 \quad (63)$$

Implementing this modified approach yields to achieve the ideal operability and transparency (according to the set α and β values). However, implementing of these modified control gains is comparatively complex than the previous method.

The position control gain C_p and force control gain C_f are set as follows.

$$C_p(s) = K_p + K_v s \quad (64)$$

$$C_f(s) = K_f \quad (65)$$

Where, K_p , K_v and K_f mean position gain, velocity gain and force gain, respectively. Moreover, the conventional and the proposed bilateral control block diagrams are shown in Figure 11 and 12 respectively.



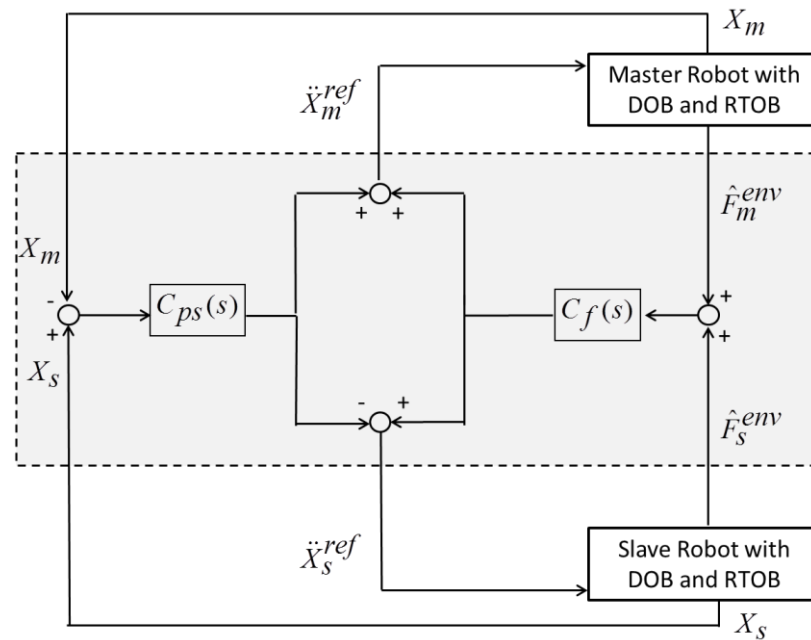


Figure 11: Conventional bilateral control system [44]

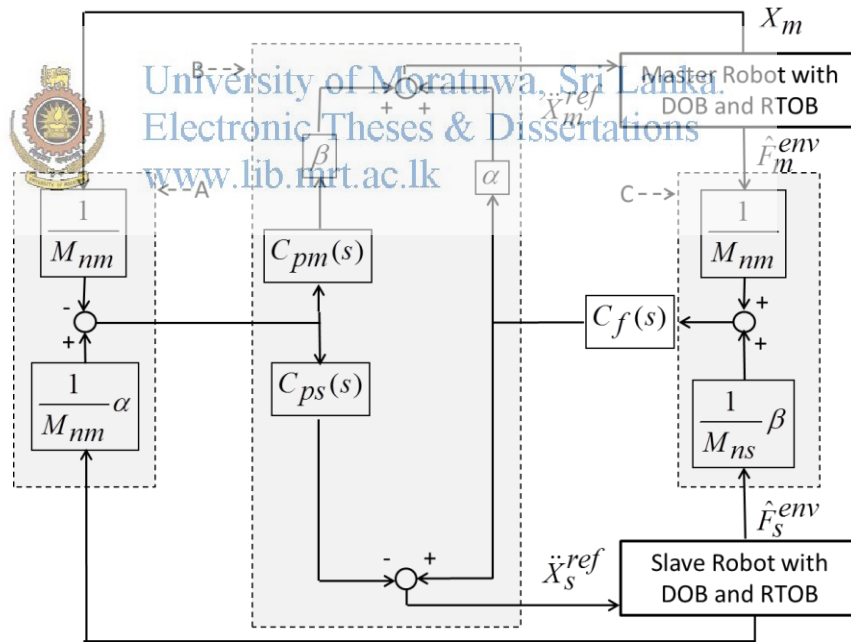


Figure 12: Proposed bilateral control system

In Figure 12, ‘A’ and ‘C’ blocks correspond to equation (43) and (44) satisfying the scaling ratios. Block ‘B’ is used to tune the system to achieve the transparency, operability and stability by adjusting the control gains.

Position control gains are defined separately for master and slave as follows.

$$C_{pm}(s) = K_p + K_{vm}s \quad (66)$$

$$C_{ps}(s) = K_p + K_{vs}s \quad (67)$$

2.5 Frequency analysis of hybrid parameters

The filters of RTOB and DOB are defined according to the below equations.

$$G_{Te} = \frac{g_{reac}}{g_{reac} + s} \quad (68)$$

$$G_{Sd} = \frac{s}{g_{dis} + s} \quad (69)$$

Where, G_{Te} is the low pass filter of RTOB and G_{Sd} is the high pass filter of equivalent acceleration disturbance by DOB. Here, g_{reac} and g_{dis} represent cut-off frequency of RTOB and DOB, respectively.

Using the above equations, the hybrid parameters of the proposed control system can be obtained as follows.

$$H_{11} = \frac{M_{nm}^2 s^2 U(s)}{D(s)} \quad (70)$$

$$H_{12} = \frac{M_{nm} (G_{Te} C_f \beta U(s) + G_{Sd} V(s))}{M_{ns} D(s)} \quad (71)$$

$$H_{21} = \frac{G_{Te} C_f \alpha \frac{M_{nm}}{M_{ns}} U(s) + G_{Sd} W(s)}{D(s)} \quad (72)$$

$$H_{22} = \frac{G_{Sd} \frac{1}{M_{ns}} I(s)}{D(s)} \quad (73)$$

Where,

$$U(s) = s^2 + (\alpha C_{ps}(s) + \beta C_{pm}(s)) \frac{1}{M_{nm} M_{ns}} \quad (74)$$

$$V(s) = M_{nm} (s^2 + \beta \frac{1}{M_{nm} M_{ns}} C_{pm}(s)) \quad (75)$$

$$W(s) = M_{nm}(s^2 + \alpha \frac{1}{M_{nm}M_{ns}} C_{ps}(s)) \quad (76)$$

$$I(s) = G_{Te} C_f (\frac{M_{nm}}{M_{ns}} \alpha + \beta) + G_{Sd} M_{nm} \quad (77)$$

$$D(s) = G_{Te} C_f U(s) + G_{Sd} \frac{1}{M_{nm}} C_{ps}(s) \quad (78)$$

2.6 Stability

The transfer function from master side force F_m to master side position X_m can be obtained from (30) as,

$$\frac{X_m}{F_m} = \frac{H_{21} + H_{22}Z_e}{H_{11} + H_{12}Z_e} \quad (79)$$

The parameters in Table 1 were used for analysis. The frequency response of the system is shown in Figure 13. To check the accuracy of parameter identification, simulation of frequency response was conducted. From Figure 13, it could be concluded that the result of identification is valid. In this analysis, the environment impedance is assumed $Z_e = 3500 + 10s$ N/m as a spring damper system.



University of Moratuwa, Sri Lanka.
Electronic Theses & Dissertations
www.lib.mrt.ac.lk

The position and force gains which are adjusted for a tuned system are fixed as 172000 and 7.73, respectively.

Table 1: System parameters used for analysis

Symbol	Description	Value
M_{nm}	Nominal mass of the master	0.3 kg
M_{ns}	Nominal mass of the slave	0.1 kg
α	Position scaling factor	2
β	Force scaling factor	2
g_{dis}	Cut-off frequency of DOB	700 rad/s
g_{reac}	Cut-off frequency of RTOB	700 rad/s
K_p	Position gain	8600 s ⁻²

K_{vm}	Velocity gain	41.47 s^{-1}
K_{vs}	Velocity gain	101.59 s^{-1}
K_f	Force gain	1.16

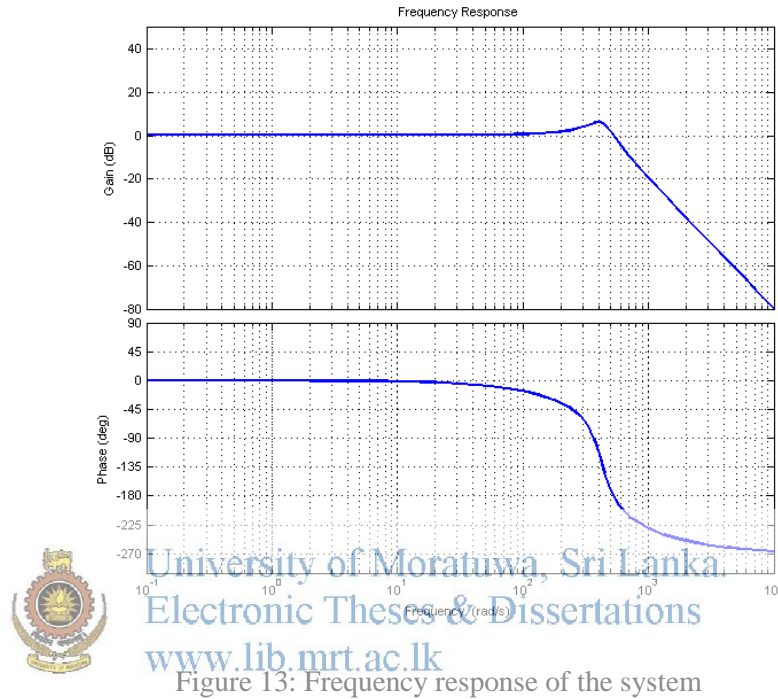


Figure 13: Frequency response of the system

The designed system perfectly follows phase and gain responses up to 10 rad/s. However, the system performance closely follows ideal responses up to 100 Hz. According to the frequency response, the system becomes marginally stable at its natural frequency of 410 Hz.

The bode plot of operability and transparency can be plotted from below equations, and shown in Figure 14. The definitions for operability and transparency can be obtained as follows from (31) and (32).

$$P_r = \frac{H_{12}}{H_{21} + H_{22}Z_e}, \quad P_o = \frac{H_{11}}{H_{21} + H_{22}Z_e} \quad (80)$$

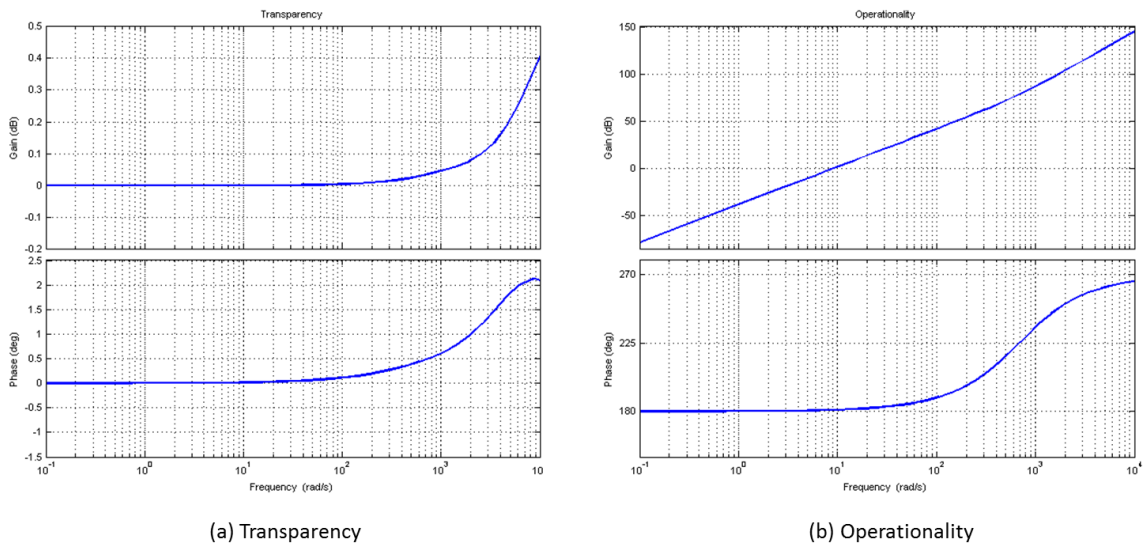


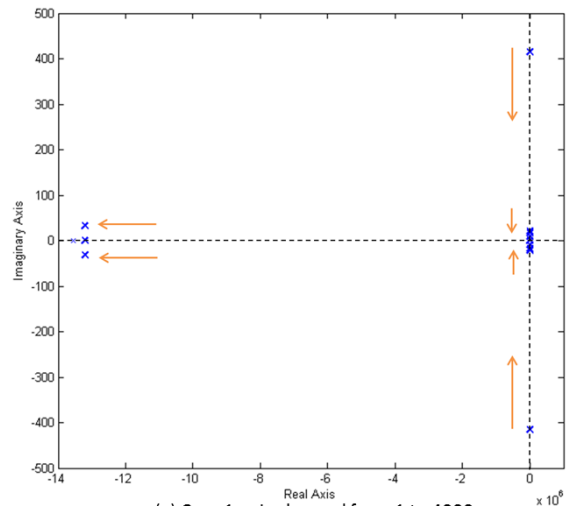
Figure 14: Phase-gain plot of transparency and operationality

In Figure 14 (a), the ideal condition for transparency $P_r = 1+0j$ was satisfied under 10 rad/s area because the gain of P_r was equal to 1.0 and there was almost no phase lag. Therefore, the operator may feel the environment impedance Z_e perfectly. However, when the frequency exceeds 100 rad/s, the ideal conditions are not satisfied.

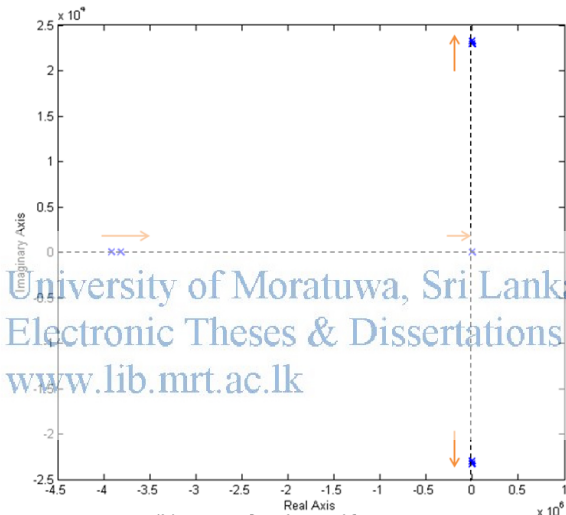
Under 1 rad/s area in Figure 14 (b), $|P_o|$ was less than 0.02 N/m. Therefore, compared to $Z_e = 3500+10s$ N/m, it can be neglected. This means there is very less additional impedance at low frequencies. When the frequency increases, the operationality also increases. This will result in that the operator feels an additional force (in addition to the reaction force) when the frequency becomes larger.

2.7 Root locus analysis

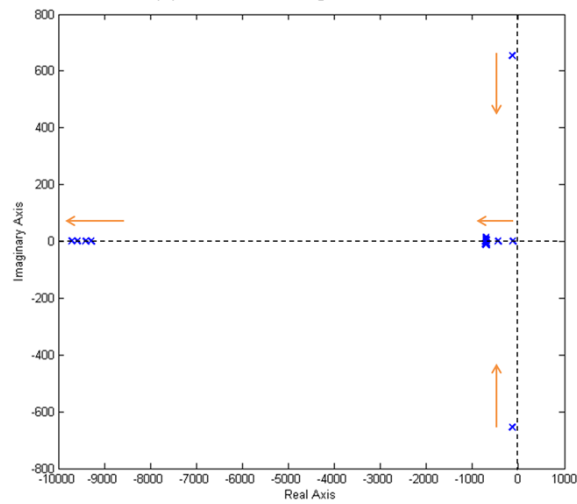
The root loci for the system were drawn from the characteristic equation ($H_{11} + H_{12}Z = 0$) of (79) for changing α , β and K_p for following three cases; case 1: α is changed from 1 to 4000, case 2: β is changed from 1 to 2000 and case 3: K_p is changed from 1: 8600. Figure 15 (a), (b), and (c) correspond to case 1, case 2 and case 3 respectively.



(a) Case 1: α is changed from 1 to 4000



(b) Case 2: θ is changed from 1 to 2000



(c) Case 3: K_p is changed from 1 to 8600

Figure 15: Root locus analysis

In Figure 15, the poles move towards right half plane when β increases. On the other hand, the poles of the system moves towards the left half plane when α or K_p become large. The gains can be tuned considering this behavior. The values presented in Table 1 represent a stable system behavior for the simulated system while satisfying above stability conditions.

2.8 Discussion

In this part of the research, scaled bilateral control system with scaling factors of the control gains is designed. These scaling factors were obtained by deriving the system based on ideal reproducibility and operability of the bilateral control system. Using the scaling factors, the control gains were scaled to appropriate values for the master and slave system according to the scaling ratio. Further, the conditions for Transparency and Operability were derived. Finally, the stability of the proposed system was analyzed using frequency responses. The bode plot diagrams drawn for transparency and operability show the operating frequency range which the proposed system can work to satisfy the ideal conditions. Pole movements of the system transfer function were analyzed for scaling factors to decide the stable range of the scaling factors.



Chapter 3

3 INERTIA ESTIMATION FOR ROBUST BILATERAL CONTROL

3.1 Introduction

The system proposed in the above section directly depends on the inertia values of the master and slave. For realizing the ideal transparency and operability, the correct estimation of inertia is necessary. In this section, a method to estimate the DC motor inertia is proposed and its applicability to accurate bilateral teleoperation is verified.

Identification of system parameters of a small DC motor is a complex and challenging task. This chapter proposes a disturbance observer (DOB) based novel Change of Inertia Observer (CIOB) to estimate the moment of inertia of a DC motor. Moment of inertia of a small DC motor is estimated using CIOB based velocity test and reaction torque observer (RTIOB) based inverse motion acceleration test, and the results are compared with conventional acceleration and deceleration motion tests. Estimated moments of inertia values are compared with the conventional methods by applying the values to a bilateral teleoperation system. Proposed method has produced better results than in the conventional methods. Proposed CIOB method of inertia estimation is much simpler and easier to use compared to conventional methods.

Identifying the real DC motor parameters is of great benefit in designing a good motion controller. There are straight forward, well-known techniques available to calculate accurate system parameters such as armature current I_a , armature resistance R_a , armature inductance L_a and torque coefficient K_t etc. However, estimating a precise motor inertia is a challenging task [45,46]. In many DC motor applications, the manufacturer given moment of inertia is considered as the actual inertia value. Sometimes, the manufacturer given value is different from the real motor inertia when different loads such as encoders are connected to the system subsequently.

Using a different inertia value may lead to erroneous system response in robotics applications such as medical robotics and aerospace automation missions where precision is important.

The nominal motor inertia J_n is provided by the manufacturer or initially calculated. However, the actual moment of inertia of the motor may be different from the nominal value due to several reasons; such as addition or removal of accessories to rotary shaft, errors in manufacturer's estimation and wear and tear effects etc. The change of inertia ΔJ represents the difference between the nominal and actual inertia values. Estimating ΔJ is the main focus in this study.

The estimated motor inertia values using CIOB based velocity test, inverse motion acceleration test and conventional acceleration and deceleration tests were applied to a bilateral control system and checked for performance in terms of the position and torque responses. Moment of inertia is one of the depending factors for the stability of the bilateral control system [47].



University of Moratuwa, Sri Lanka.
Electronic Theses & Dissertations
www.lib.mrt.ac.lk

3.2 System modeling

The following equations (81-84) can be obtained from the electrical representation of a DC motor. Where, E_b - the back emf, T_m - motor torque, K_e - back emf constant, ω - angular speed, K_t - torque coefficient and I_a - armature current.

$$V_a = L \frac{dI_a}{dt} + RI_a + E_b \quad (81)$$

$$E_b = K_e \omega \quad (82)$$

$$T_m = K_t I_a \quad (83)$$

Considering the mechanical parameters of the motor, the motor torque can be written as;

$$T_m = J \frac{d\omega}{dt} + T_f + B\omega + T_l \quad (84)$$

Where, J - motor inertia, T_f - static friction, B - viscous friction coefficient, and T_l - load torque.

The integrated disturbance observer measures and compensates the disturbances to the system and hence it can be effectively used in motion control applications of robotics [45]. The disturbance torque of the motor T_{dis} can be obtained from (85). Here, K_t is the torque coefficient, J is the inertia of the load coupled with the rotor and the subscript n is used to denote the nominal values.

$$T_{dis} = K_{tn}I_a - J_n\dot{\omega} \quad (85)$$

If the nominal motor inertia J_n varies by ΔJ and nominal torque coefficient K_{tn} varies by ΔK_t , the actual J and K_t can be represented by (86) and (87) respectively. Here, nominal torque coefficient and nominal motor inertia values are known from the manufacturer's specifications. Armature current and angular speed can easily be measured using an ammeter and an encoder respectively.

$$J = J_n + \Delta J \quad (86)$$

$$K_t = K_{tn} + \Delta K_t \quad (87)$$

$$T_{dis} = T_l + T_f + B\omega + \Delta J\dot{\omega} - \Delta K_t I_a \quad (88)$$

Disturbance torque T_{dis} in (88) consists of load torque T_l , frictional torque $T_f + B\dot{\theta}$ and torques arising from parameter variations. T_{dis} can be calculated by using the known parameters of (85). Then, the disturbance observer output is the estimated disturbance torque \hat{T}_{dis} given by (89). Where, G_{dis} is the disturbance gain.

$$\hat{T}_{dis} = \frac{G_{dis}}{(s + G_{dis})} T_{dis} \quad (89)$$

The disturbance observer calculates and estimates the reaction torque as quickly as possible. Using the disturbance feedback it could compensate for the unknown disturbances acting on the system. Furthermore, from the disturbance output, if the frictional components are measured and eliminated, then, the real reaction torque could be measured.

3.2.1 Conventional inertia estimation methods

The conventional acceleration and deceleration tests [48-50] can be modeled from their native equations as follows:

3.2.1.1 Acceleration motion test

$$\text{Motor Inertia}(J) = \frac{\text{Acceleration Torque}}{\text{Acceleration}} (\text{kgm}^2) \quad (90)$$

3.2.1.2 Deceleration motion test

This test can be performed as follows. The DC motor is switched off when it is running at its rated speed, and then, the motor speed reduces to zero from its steady speed. The dynamic torque equation for this test is given by (91). The time domain solution for (91) can be expressed as (92). Where, ω_{ss} is the steady state speed.

While the motor speed decreases from steady state speed to zero, following equations (91-93) can be derived to calculate the inertia. Where, ω_{ss} is the steady state speed and τ is mechanical time constant

$$J\dot{\omega} + T_f + B\omega = 0 \quad (91)$$

Solving differential equation (91),

$$\omega = (\omega_{ss} - \frac{T_f}{J})e^{-(B/J)t} \quad (92)$$

$$J = B\tau \quad (93)$$

3.2.2 Proposed change of inertia observer

Disturbance observer can be used not only for disturbance compensation but also to estimate the change of motor inertia. The disturbance observer is able to estimate the torque variation caused due to the change of the moment of inertia. This estimation is done without using any torque sensor and only by identifying the internal disturbance of the system [51].

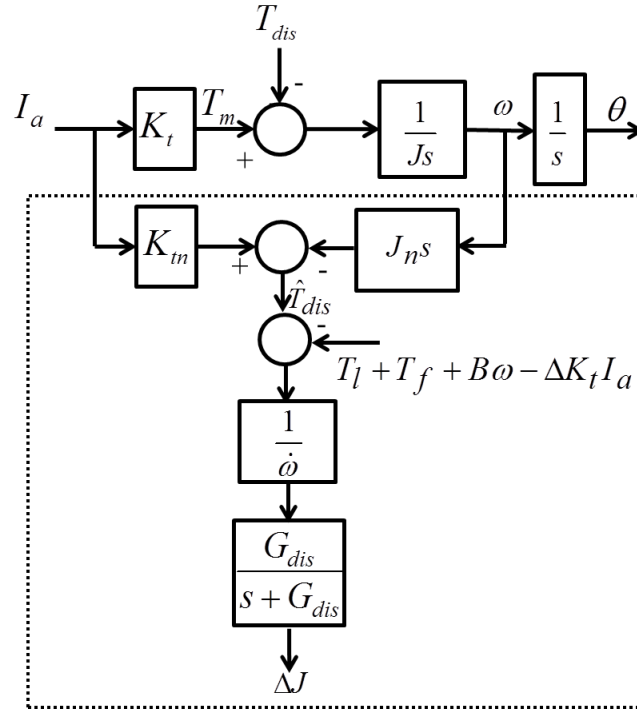


Figure 16: Change of inertia observer.

Disturbance observer output T_{dis} is calculated using known parameters (K_m, I_a, J_n and $\dot{\omega}$) of (85). A low pass filter with disturbance gain G_{dis} is used to suppress noise components added by differentiation block $J_n s$. Load torque, frictional torque and torque due to motor constant variation are removed from the DOB output. Then, the DOB output consists of only the torque components of the moment of inertia variation. Therefore, the CIOB output yields to the change of inertia ΔJ .

The moment of inertia of the DC motor is calculated with this novel tool. This is a disturbance observer based sensor used to measure the variation of the motor inertia ΔJ . The total disturbance to the system is given by (88).

The load torque T_l can be made zero by conducting the test in the no load condition. The variation of the motor torque coefficient is usually insignificant or it can be easily calculated [52]. Usually, ΔK_t is considered to be insignificant, then the total disturbance can be expressed by (94).

$$T_{dis} = T_f + B\omega + \Delta J\dot{\omega} \quad (94)$$

The friction components are separately calculated and compensated to the system as shown in Figure 16. Therefore, the CIOB output represents the estimated change of inertia of the motor ΔJ . This tool can be effectively used to find the real inertia value of the system. The ΔJ variation can be added or subtracted from the nominal motor inertia and it is possible to fine tune the system by analyzing the torque response graphs as shown in Figure 17 (a) and (b), for positive and negative ΔJ values respectively. The dotted lines in Figure 17 (a) and (b) represent the torque variation when the applied motor inertia value equals the actual value.

In this test, the motor was kept upright fixed position (vertically mounted). Then, the motor is accelerated from zero to a constant velocity. The acceleration is kept constant over the accelerating period. The torque response of this test can be further elaborated with the aid of Figure 17. Figure 17 (a) and (b) are graphical explanations for (94). The deviation of the moment of inertia from the nominal moment of inertia is represented by the shaded areas of Figure 17 (a) and (b). In this proposed CIOB test, ΔJ can be identified from the CIOB output and from the torque versus time plot. Then, by adjusting the nominal moment of inertia by ΔJ , the torque response becomes dependent only on friction components.

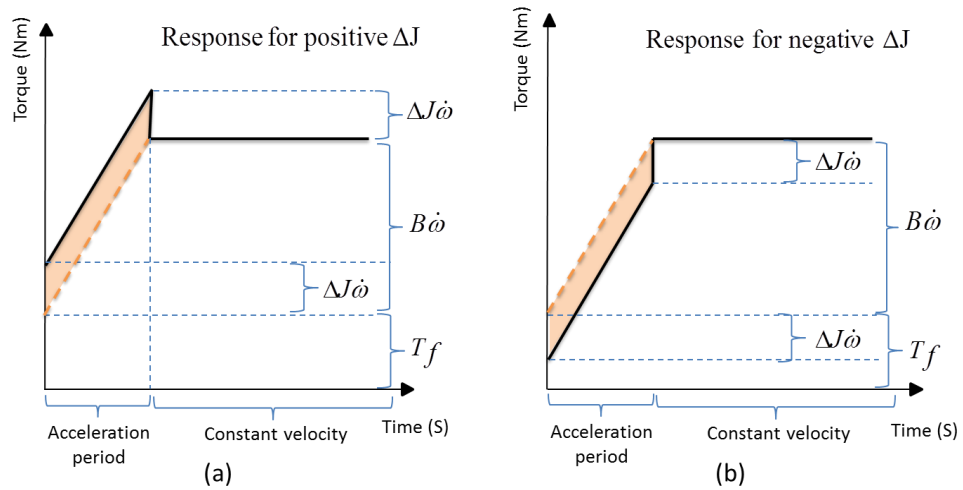


Figure 17: Torque responses. (a) Torque responses for positive ΔJ . (b) Torque responses for negative ΔJ .

3.2.3 Inverse motion acceleration test

In this approach, RTOB is used as a torque sensor. The calculated values for motor parameters (K_t , T_f and B) are used for this test. A DOB based robust velocity controller is used to achieve accurate velocity responses [53]. The test was conducted by reversing the motor direction with controlled deceleration while it was running at steady state speed. The immediate change of the direction is governed by the controller. As shown in Figure 18, the motor acceleration to the opposing direction starts at t_1 and ends at t_2 . At t_2 , the motor comes to a steady state speed of the new direction. This direction variation results in a variation of torque. Motor inertia is directly estimated using the variation of torque.

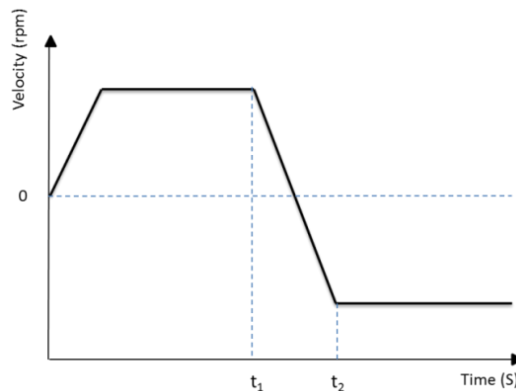


Figure 18: Velocity response of the inverse motion acceleration test.

The RTOB output of the inverse motion acceleration test, \hat{T}_{dis} consists of only the change of motor inertia. The other disturbance components are known and eliminated at the RTOB.

$$\hat{T}_{dis} = \Delta J \dot{\omega} \quad (95)$$

By combining (88) and (95), \hat{T}_{dis} can be expressed in (96).

$$\hat{T}_{dis} = (J - J_n) \dot{\omega} \quad (96)$$

Then, in (97) the expression is integrated for the time interval t_1 to t_2 .

$$\int_{t_1}^{t_2} \hat{T}_{dis} dt = (J - J_n) [\omega(t_2) - \omega(t_1)] \quad (97)$$

Motor inertia J can be calculated from the right hand side known parameters of (98).

$$J = J_n + \frac{1}{[\omega(t_2) - \omega(t_1)]} \int_{t_1}^{t_2} \hat{T}_{dis} dt \quad (98)$$

In the inverse motion acceleration test, the friction components are compensated for, together with other disturbances. The friction components are calculated by conducting the unidirectional constant velocity test [53]. But in this test, the motor direction is reversed and the region of operation consists of the frictional effects for both directions of the DC motor. Normally, the friction components are different for both motor directions, and friction non-linearity also affects the friction estimation. Therefore, the compensated friction components may not be accurate.

3.3 Results and discussion

3.3.1 Selecting bilateral control for inertia verification

Bilateral control is one of the most widely used teleoperation technologies today [45]. Its controller is based on realization of law of action and reaction between the operator and the environment. It controls the master and the slave sides from the responses of the slave and master sides respectively [45,53]. As far as the transparency and operability improvement of the bilateral control is concerned,

identifying the accurate system parameters is an essential task [54]. Amongst the system parameters, identifying the actual moment of inertia of the DC motor is not straight forward. When the manufacturer provides a nominal inertia value that does not represent the actual inertia of the motor, the system will produce undesirable responses. In a bilateral control system, one to one position and torque responses are expected. Here, the bilateral teleoperation system is used to verify the accuracy of the inertia values calculated from the four tests discussed above.

The bilateral teleoperation system used for this experiment consists of two identical modules called master and slave. A module is modeled in the Matlab Simulink environment, and the frequency responses are analyzed for position response by changing the inertia value of the motor from 0.00001 – 0.00009 kgm². This simulation was done to identify the effect of the changing motor inertia of the DC motor. According the simulation results in Figure 19, there is a significant change in the system bandwidth when the moment of inertia is changed within this considered range. Therefore, it is important to identify the exact inertia value of the motor to achieve the desired system response. Inability to identify the correct motor inertia will lead the system to an undesired state.



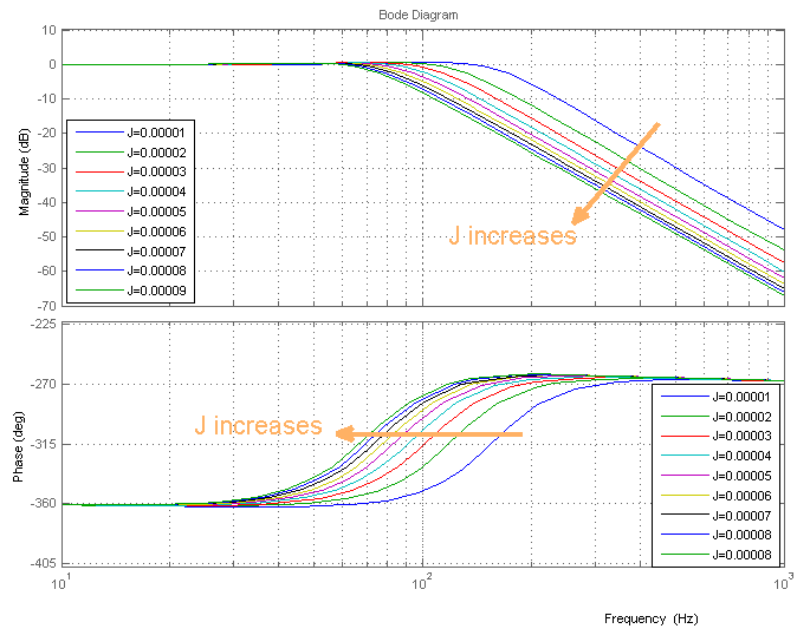


Figure 19: Frequency response of the master or slave system for position control with different motor inertia values.

3.3.2 Experimental setup

The hardware arrangement of the experiment is shown in Figure 20. The specifications of the motor are listed in table 2. The motor is driven by a PWM based motor driver with a driver IC (DRV8432 by Texas Instrument) which can carry current up to 14A with 24A peak load. The PWM signals are generated by the processor. An encoder is coupled to the motor to sense the position.



Figure 20: Bilateral test platform

All computations are written in C language under real time operating system (RTOS) with a sampling time of $100\mu\text{s}$. Time critical main control program was invoked in every $100\mu\text{s}$, while the data writing task is given the lowest priority.



University of Moratuwa, Sri Lanka.
Electronic Theses & Dissertations
www.theses.dlib.lk

Parameter	Value	Unit
Rated output	0.2	kW
Rated/max. torque	20.5/169.5	Ncm
Encoder resolution	2500	Pulses/rev

3.3.3 Estimation of motor inertia experimentally

The moment of inertia of the DC motor is estimated by using four tests for comparison purposes; conventional acceleration and de-acceleration tests, CIOB based velocity test and reaction torque observer (RTOB) based inverse motion acceleration test. The estimated inertia values from each test are listed in Table 3. According to the obtained results, it is shown that CIOP test output gives the best estimated inertia value.

3.3.3.1 Acceleration motion test results

In this test, the torque is recorded at the controller itself. Equation (82) is used to calculate the motor inertia and the resulting inertia value is 0.000051 kgm^2 . The corresponding velocity response of the acceleration motion test is presented in Figure 21 (a).

3.3.3.2 Deceleration motion test results

Velocity response of deceleration motion test is shown in Figure 21 (b). The calculated motor inertia in the deceleration motion test by using (85) is 0.000032 kgm^2 .

3.3.3.3 Change of inertia motion test results

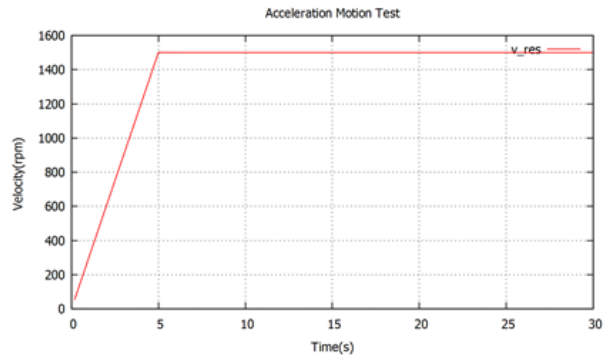
The velocity and torque responses of CIOB based constant velocity test are shown in Figure 21 (c) and (22) respectively. The estimated moment of inertia, by using (86) and Figure 22 is 0.000072 kgm^2 . Torque response of Figure 22 follows the shape of torque response for positive ΔJ of Figure 17 (a). However, during the acceleration time the torque response is not linear and instead it takes a slightly curved shape. This is due to the low pass filter at DOB, but it does not affect the estimation of ΔJ . Further, system non linearity, motor saturation and estimation errors may be the causes for this outcome.

3.3.3.4 Inverse motion acceleration test results

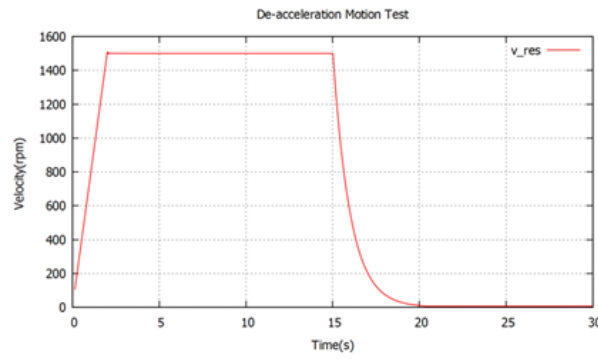
In this test, the motor inertia is calculated from (90). Velocity response of the test is displayed in Figure 21 (d). The calculated motor inertia is 0.000091 kgm^2 .

Table 3: Inertia estimation results

Test	Estimated Inertia value/ kgm^2
Acceleration motion test	0.000051
Deceleration motion test	0.000032
Change of inertia motion test	0.000072
Inverse motion acceleration test	0.000091



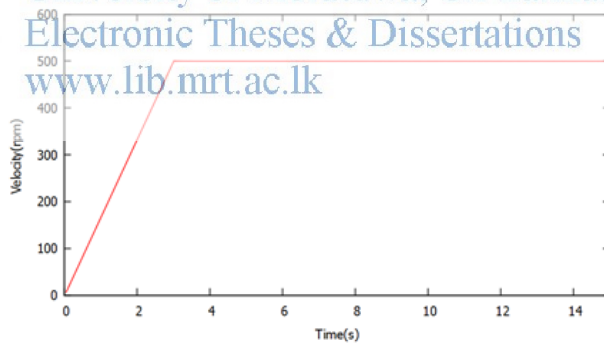
(a)



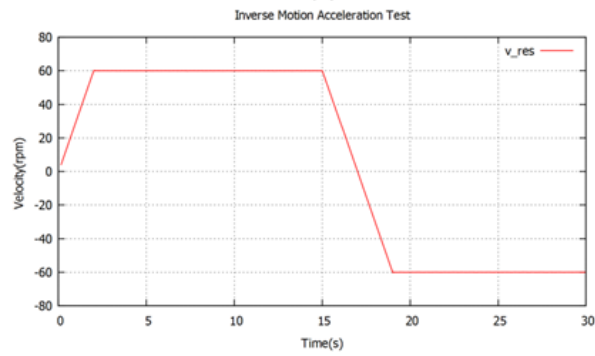
(b)



University of Moratuwa, Sri Lanka.
Electronic Theses & Dissertations
www.lib.mrt.ac.lk



(c)



(d)

Figure 21: Velocity responses

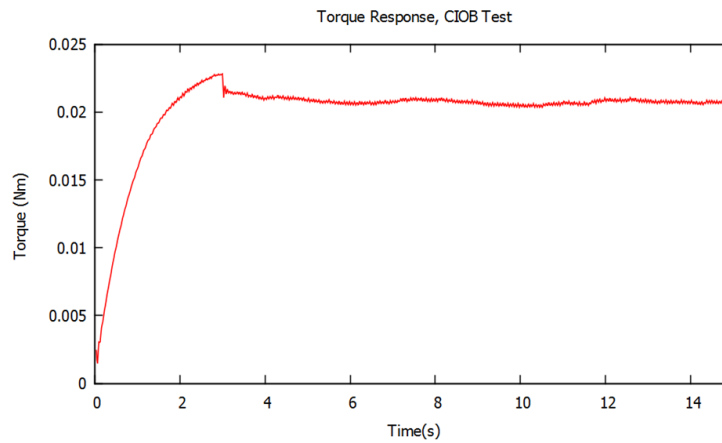


Figure 22: Torque response of CIOB test

3.3.4 Validating the results with bilateral teleoperation

The four motor inertia values calculated from the four tests described in the modeling section are applied to a bilateral control system and tested. Bilateral control system is operated under free and contact motions, and position and torque responses are plotted against time for each inertia value. While doing this series of experiments, all the parameters except motor inertia of the master or slave are kept constant for comparison purposes.

Figure 23 (a)–(h) represent the position and torque responses of the bilateral controller for the four different moments of inertia values. In the bilateral control system, the position response of the slave device should follow that of the master device. The torque response of slave device should be the mirror image of that of the master device in the graphical representation.

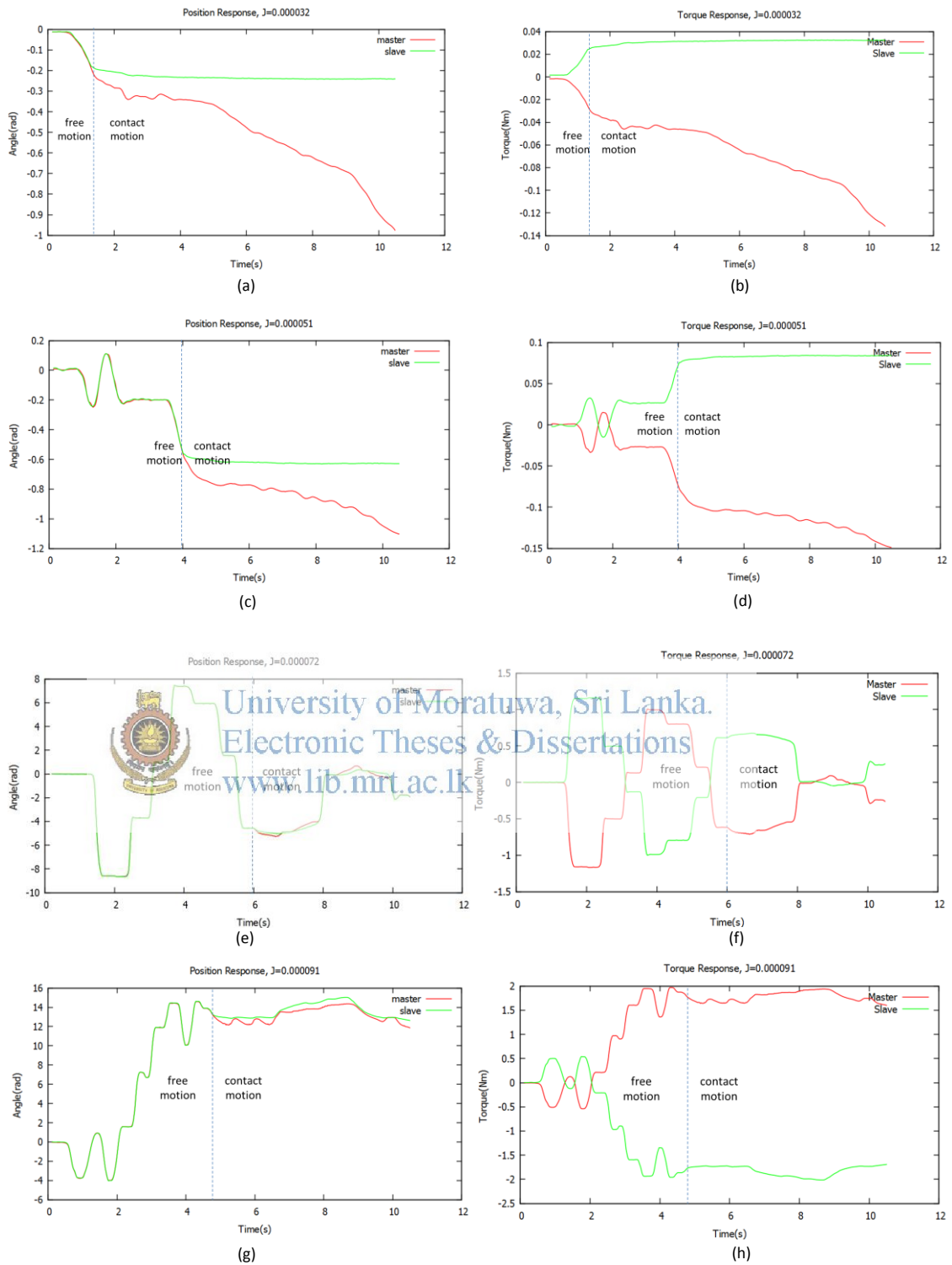


Figure 23: Position and torque responses. (a),(b): acceleration motion test (c),(d): deceleration motion test (e),(f): CIOB test (g),(h) inverse motion acceleration test

The motion profiles in Figure 23 were achieved by applying manual force and position inputs to the bilateral platform. The objective of this experiment is to identify the most accurate force and position responses in bilateral controls. The figures corresponding to the deceleration motion test (Figure 23 (c) and (d)) do not show the desired system performance. Figure 23 (a) and (b) show improved performances in position and torque responses for the moment of inertia calculated by acceleration motion test compared to the deceleration motion test.

However, the system responses for the moment of inertia values of inverse motion acceleration test and CIOB-test, as shown in Figure 23 (e)-(h), are satisfactory representations for the bilateral teleoperation. Figure 23 (e) and (f) show the best performances among these responses. The moment of inertia estimated from CIOB test gives the best performance in the bilateral control system (inertia value of 0.000072 kgm^2). The position and torque responses of the bilateral control show the minimum errors in this case, and hence the calculated moment of inertia using CIOB test matches to the bilateral control system. Position is the dominant characteristic under free motion. Position responses of Figure 22 show that the position error is very small for the proposed methods.

3.4 Conclusion

In this chapter, a novel method of estimating the moment of inertia of a small DC motor is proposed. In this research, no torque sensors are used for the proposed method. DOB and its variant RTOB are used to attain robustness and to measure the torque respectively. The proposed method, CIOB is a tool that provides the error of the nominal motor inertia such that it can be used as a tool to derive the actual inertia value. This tool can be used in motion control applications to adjust the moment of inertia parameter to its real value. The test results are compared with conventional test outputs. The estimated moment of inertia values of these four tests are separately applied to conventional bilateral control system and the position and torque responses of the bilateral teleoperation were analyzed. The experimental results

prove the viability of the proposed method. This method can be used to estimate the motor inertia of small DC motors and hence improve the transparency and operability of bilateral teleoperation systems.



University of Moratuwa, Sri Lanka.
Electronic Theses & Dissertations
www.lib.mrt.ac.lk

Chapter 4

4 CONCLUSIONS

Scaling is a technique used to transfer the dynamic motion properties of a remote device (slave robot) to the operator (master robot) or vice versa. This is a challenging task in terms of force, position, power, and impedance scaling approaches when master and slave manipulators are dissimilar. Teleoperation using scaling methods is a popular topic in motion control field, and many research papers are written on different scaling methods.

This research addressed the most important two aspects of the bilateral control system: transparency and operability improvements. The proposed design consisted on two main parts: Transparency and Operability improvements in bilateral teleoperation and inertia estimation for robust bilateral control. In the first part of the research, a bilateral control system was proposed with the scaling factors derived in terms of the master and slave inertias. Further, this concept was improved by introducing arbitrary force and position scaling factors in addition to the nominal inertias. The main objectives of bilateral teleoperation are to achieve the ideal transparency and operability conditions. In the proposed design, a condition for ideal transparency and operability was introduced for a bilateral teleoperation system which performs force and position scaling tasks. The system performance was analyzed considering the system frequency responses and root loci. This proposed system was simulated and verified its performance using the standard stability analysis tools.

In the second part of the research, a method to estimate the accurate master and slave inertias was proposed. Estimating the correct inertia values is very important to achieve the desired transparency and operability in bilateral control. In this approach, a method to effectively estimate the DC motor inertia value was proposed. The estimated inertia value obtained from the proposed method was applied on the

real bilateral platform. The validity of the proposed method was experimentally verified comparing with the conventional methods.

It can be concluded that the transparency and operability conditions for scaled bilateral teleoperation can be achieved to a certain extent on the theoretical grounds. However, it is practically not possible to achieve both ideal transparency and operability together. The derived method also proves this popular transparency and operability relationship. Further, estimating the correct inertia values of the master and slave robots is very important to achieve the desired transparency and operability conditions. The proposed method to estimate the DC motor inertia helps to further improve the bilateral control performances.

4.1 Recommendation for future developments

Many of the real world teleoperation systems or teleoperation applications do not use one-to-one force and position following approaches. Scaling in terms of force, position, power, impedance and sometimes time provides humans to apply their skills in a various industrial missions. These applications range from extending human operator's skills in minimally invasive surgeries to outer orbit space applications. As discussed and stated in this thesis, a number of scaling approaches in bilateral teleoperations have been developed for different application areas. Many different control strategies have been presented to efficiently handle the teleoperation tasks. There are effective and promising studies to address the issues related to force, position, power and impedance scaling formulations. However, so far, the time scaling in bilateral teleoperation is not a matured research area. Time delay introduced by the communication channel can cause deterioration in system response and make the system unstable easily. Consequently, it is vital to focus the future bilateral scaling experiments on robust time scaling and compensation methods.

5 REFERENCES

- [1] Hokayem, Peter F., and Mark W. Spong. "Bilateral teleoperation: An historical survey." *Automatica* 42.12 (2006): 2035-2057.
- [2] Lasnier, Antoine, and Toshiyuki Murakami. "Workspace based force sensorless bilateral control with multi-degree-of-freedom motion systems." *Advanced Motion Control, 2010 11th IEEE International Workshop on*. IEEE, 2010.
- [3] Hasegawa, Shoichi, and Makoto Sato. "Real-time Rigid Body Simulation for Haptic Interactions Based on Contact Volume of Polygonal Objects." *Computer Graphics Forum*. Vol. 23. No. 3. Blackwell Publishing, Inc, 2004.
- [4] Tsumaki, Yuichi, and Masaru Uchiyama. "A model-based space teleoperation system with robustness against modeling errors." *Robotics and Automation, IEEE International Conference on*. Vol. 2. IEEE, 1997.
- [5] Kazerooni, Hami, Ryan Steger, and Lihua Huang. "Hybrid control of the berkeley lower extremity exoskeleton (bleex)." *The International Journal of Robotics Research* 25.5-6 (2006): 561-573.
- [6] R.S. Mosher, *From Handiman to Hardiman*. Society of Atomotive Engineers Transactions, 76:588-597, 1967, Report Number 670088
- [7] Colgate, J. Edward. "Power and impedance scaling in bilateral manipulation." *Robotics and Automation, IEEE International Conference on*. IEEE, 1991.
- [8] Sheridan, Thomas B. *Supervisory control: Problems, theory and experiment for application to human-computer interaction in undersea remote systems*. MASSACHUSETTS INST OF TECH CAMBRIDGE MAN-MACHINE SYSTEMS LAB, 1982.
- [9] Sakaki, Taisuke, and Susumu Tachi. "Impedance Scaling of a Tele-Existence Master-Slave Manipulation System by Using Similarity Transformation." (1992).
- [10] Raju, G. Jagannath. *Operator adjustable impedance in bilateral remote manipulation*. Diss. Massachusetts Institute of Technology, 1988.
- [11] Colgate, J. Edward. "Robust impedance shaping telemanipulation." *Robotics and Automation, IEEE Transactions on* 9.4 (1993): 374-384.
- [12] Salcudean, Septimiu E., S. Ku, and G. Bell. "Performance measurement in scaled teleoperation for microsurgery." *CVRMed-MRCAS 97*. Springer-Verlag Heidelberg, 1997.
- [13] Salcudean, S. E., and Joseph Yan. "Towards a force-reflecting motion-scale system for microsurgery." *Robotics and Automation, IEEE International Conference on*. IEEE, 1994.
- [14] Watanabe, G., and N. Ishikawa. "[Da Vinci Surgical System]." *Kyobu geka. The Japanese journal of thoracic surgery* 67.8 (2014): 686-689.
- [15] Lowe, M. Patrick. "Da Vinci Surgical System.", http://roboticsurgery.nm.org/uploads/2/4/4/3/24430153/northwestern_robotics_booklet.doc, accessed in Oct. 2014.
- [16] Kazerooni, Homayoon. "Extender: a case study for human-robot interaction via transfer of power and information signals." *Robot and Human Communication, 2nd IEEE International Workshop on*. IEEE, 1993.
- [17] Anderson, Robert J., and Mark W. Spong. "Asymptotic stability for force reflecting teleoperators with time delay." *The International Journal of Robotics Research* 11.2 (1992): 135-149.
- [18] Colgate, J. Edward. "Robust impedance shaping telemanipulation." *Robotics and Automation, IEEE Transactions on* 9.4 (1993): 374-384.
- [19] Colgate, J. Edward. "Robust impedance shaping via bilateral manipulation." *American Control Conference, IEEE, 1991*.
- [20] Hannaford, Blake. "Stability and performance tradeoffs in bi-lateral telemanipulation." *Robotics and Automation, IEEE International Conference on*. IEEE, 1989.
- [21] Brooks, Thurston L. "Telerobotic response requirements." *Systems, Man and Cybernetics, Conference Proceedings.*, IEEE International Conference on. IEEE, 1990.
- [22] Hannaford, Blake. "A design framework for teleoperators with kinesthetic feedback." *Robotics and Automation, IEEE Transactions on* 5.4 (1989): 426-434.
- [23] Niemeyer, Günter, and J-JE Slotine. "Stable adaptive teleoperation." *Oceanic Engineering, IEEE Journal of* 16.1 (1991): 152-162.
- [24] Niemeyer, Günter, and Jean-Jacques E. Slotine. "Telemanipulation with time delays." *The International Journal of Robotics Research* 23.9 (2004): 873-890.
- [25] Niemeyer, Günter, and J-JE Slotine. "Towards force-reflecting teleoperation over the internet." *Robotics and Automation, IEEE International Conference on*. Vol. 3. IEEE, 1998.
- [26] Aziminejad, Arash, et al. "Transparent time-delayed bilateral teleoperation using wave variables." *Control Systems Technology, IEEE Transactions on* 16.3 (2008): 548-555.

- [27] Haddadi, Amir. "Stability, Performance, and Implementation Issues in Bilateral Teleoperation Control and Haptic Simulation Systems.", PhD thesis, (2012).
- [28] Susa, Shigeru, et al. "Transmission of force sensation by micro-macro bilateral control with scaling of control gains." *Advanced Motion Control, AMC'08. 10th IEEE International Workshop on. IEEE*, 2008.
- [29] Zhu, Ming, and Septimiu E. Salcudean. "Achieving transparency for teleoperator systems under position and rate control." *Intelligent Robots and Systems 95.'Human Robot Interaction and Cooperative Robots', IEEE/RSJ International Conference on. Vol. 2. IEEE*, 1995.
- [30] Lawrence, Dale A. "Designing teleoperator architectures for transparency." *Robotics and Automation, IEEE International Conference on. IEEE*, 1992.
- [31] Lawrence, Dale A. "Stability and transparency in bilateral teleoperation." *Robotics and Automation, IEEE Transactions on* 9.5 (1993): 624-637.
- [32] Zhu, Wen-Hong, S. E. Salcudean, and Ming Zhu. "Experiments with transparent teleoperation under position and rate control." *Robotics and Automation, IEEE International Conference on. Vol. 3. IEEE*, 1999.
- [33] Salcudean, Septimiu E., et al. "Transparent bilateral teleoperation under position and rate control." *The International Journal of Robotics Research* 19.12 (2000): 1185-1202.
- [34] Misra, Sarthak, and Allison M. Okamura. "Environment parameter estimation during bilateral telemanipulation." *Haptic Interfaces for Virtual Environment and Teleoperator Systems, 14th Symposium on. IEEE*, 2006.
- [35] Salcudean, S. E., et al. "Bilateral matched impedance teleoperation with application to excavator control." *Control Systems, IEEE* 19.6 (1999): 29-37.
- [36] Kosugi, Takahiro, and Seiichiro Katsura. "Experimental investigation of variable scaled bilateral control." *Human System Interactions (HSI), 4th International Conference on. IEEE*, 2011.
- [37] Khan, Shahzad, Asif Sabanovic, and Ahmet Ozcan Nergiz. "Scaled bilateral teleoperation using discrete-time sliding-mode controller." *Industrial Electronics, IEEE Transactions on* 56.9 (2009): 3609-3618.
- [38] Tsuji, Toshiaki, Kenji Natori, and K. Ohnishi. "A controller design method of bilateral control system." *EPE JOURNAL* 16.2 (2006): 22.
- [39] Ishii, Ena, Hiroaki Nishi, and Kouhei Ohnishi. "Improvement of performances in bilateral teleoperation by using FPGA." *Industrial Electronics, IEEE Transactions on* 54.4 (2007): 1876-1884.
- [40] Mizoguchi, Takahiro, Takahiro Nozaki, and Kouhei Ohnishi. "Scaling bilateral controls with impedance transmission using transfer admittance." *Advanced Motion Control (AMC), 2012 12th IEEE International Workshop on. IEEE*, 2012.
- [41] Funabiki, S., Fukushima, T., "Current commands for high-efficiency torque control of DC shunt motor," in *IEE Proceedings B, Electric Power Applications*, vol. 138, no. 5, pp. 227-332, Sept-1991.
- [42] AM Harsha S Abeykoon, and Kouhei Ohnishi, "Improvement of Tactile Sensation of a Bilateral Forceps Robot by a Switching Virtual Model," *Trans. Advanced Robotics*, vol. 22, no. 8, pp. 789-806, Aug-2008.
- [43] Iida, W.; Ohnishi, K., "Reproducibility and operationality in bilateral teleoperation," *Advanced Motion Control, AMC '04. The 8th IEEE International Workshop on*, vol., no., pp.217,222, 25-28 March 2004
- [44] Iwata, S.; Matsumi, Y.; Ohnishi, K., "Two-step scaling micro-macro bilateral control using double master slave system," *Industrial Electronics Society, IECON - 39th Annual Conference of the IEEE*, vol., no., pp.4300,4305, 10-13 Nov. 2013
- [45] Ohnishi, K., Katsura, S., Shimono, T., "Motion Control for Real-World Haptics," *IEEE Trans. Ind. Electron. Magazine*, vol.4, no. 2, pp. 16-19, June 2010.
- [46] Murakami, T., Ohnishi, K., "Observer-based motion control-application to robust control and parameter identification," in *Proc. Asia-Pacific Workshop on AMC*, 1993, pp.1-6.
- [47] Sandra Hirche, Manuel Ferre, Jordi Barrio, Claudio Melchiorri, Martin Buss, "Bilateral Control Architectures for Telerobotics", *Springer Tracts in Advanced Robotics*, Springer Berlin Heidelberg, pp 163-176, 2007.
- [48] C.Ganesh, B.Abhi, V.P.Anand, S.Aravind, R.Nandhini, and S.K.Patnaik, "DC Position Control System-Determination of Parameters and Significance on System Dynamics," *ACEEE Trans. J. Electrical and Power Eng.*, vol.3, no.1, pp.1-5, Feb-2012.
- [49] Robet, P.P., Gautier, M., Jubien, A., Janot, A., "Global identification of mechanical and electrical parameters of DC motor driven joint with a fast CLOE method," in *Proc. IEEE/ASME Advanced Intelligent Mechatronics (AIM)*, 2013, pp.1205-1210.
- [50] Saab, S.S., Kaed-Bey, R.A., "Parameter identification of a DC motor: an experimental approach," in *Proc. 8th IEEE Electronics, Circuits and Systems (ICECS)*, 2001, pp.981-984.

-
- [51] AM Harsha S Abeykoon, Kouhei Ohnishi, "Improvement of Tactile Sensation of a Bilateral Forceps Robot by a Switching Virtual Model," *Trans. Advanced Robotics*, vol. 22, no. 8, pp. 789-806, Aug-2008.
- [52] C.Ganesh, B.Abhi, V.P.Anand, S.Aravind, R.Nandhini, and S.K.Patnaik, "DC Position Control System-Determination of Parameters and Significance on System Dynamics," *ACEEE Trans. J.Electrical and Power Eng.*, vol.3, no.1, pp.1-5, Feb-2012.
- [53] Hasala R Senevirathne, AM Abeykoon, M Branesh Pillai, "Disturbance rejection analysis of a disturbance observer based velocity controller," in *Proc. 6th IEEE Information and Automation for Sustainability (ICIAfS)*, 2012, pp. 59-64.
- [54] Ohishi, K., Nakao, Masato., Ohnishi, K., and Miyachi, Kunio, "Microprocessor-Controlled DC Motor for Load-Insensitive Position Servo System," *IEEE Trans. Ind. Electron.*, vol. IE-34, no. 1, pp.44-49, Feb-1987.
- [55] Ohnishi, K., Shibata, M., and Murakami, T, "Motion control for advanced mechatronics," *IEEE/ASME Trans. Mechatronics*, vol.1, no.1, pp.56-67, Mar-1996.
- [56] Saito, E., and Katsura, S., "A filter design method in disturbance observer for improvement of robustness against disturbance in time delay system," in *Proc. IEEE Industrial Electronics (ISIE)*, 2012, pp. 1650-1655.



University of Moratuwa, Sri Lanka.
Electronic Theses & Dissertations
www.lib.mrt.ac.lk

6 APPENDIX

Appendix I

```
% tuned T/F for operationality and transparency
```

```
s = tf('s');
Mnm=0.3;
Mns=0.1;
a=2;
b=2;
g_dis=700;
g_reac=700;
Kp=8600;
Kf=1.16;
```

```
Gte=g_reac/(g_reac+s);
Gsd=g_dis/(g_dis+s);
Kvm=41.47 %2*(Mns*Kp/b)^(0.5)
Kvs=101.59 %2*(Mnm*Kp)^(0.5)
Cpm=Kp+Kvm*s;
Cps=Kp+Kvs*s;
Cf=Kf;
```

```
U=s^2+(a*Cps+b*Cpm)/(Mnm*Mns);
V=Mnm*(s^2+b*Cpm/(Mnm*Mns));
W=Mnm*(s^2+a*Cps/(Mnm*Mns));
I=Gte*Cf*((Mnm/Mns)^a+b)+Gsd*Mnm;
D=Gte*Cf*U+Gsd*Cps*W;
H11=(Mnm^2*s^2*U)/D;
H12=Mnm*(Gte*Cf*b*U+Gsd*V)/(Mns*D);
H21=(Gte*Cf*a*(Mnm/Mns)*U+Gsd*W)/D;
H22=Gsd*I/(Mns*D);
```

```
Ke=3600;
De=8;
Ze=Ke+s*De;
```

```
opts = bodeoptions;
opts.FreqUnits = 'rad/s';
opts.Grid='on';
opts.Xlim=[0.1,10000];
```

```
T1=H21/(H11+H12*Ze); %master system transfer fn
```

```
Figure (1)
bodeplot (T1,opts);
Po=H11/(H21+H22*Ze);
Pr=H12/(H21+H22*Ze);
Figure (2)
bodeplot (Pr,opts)
Figure (3)
bodeplot (Po,opts)
```

Appendix II

```
% tuned T/F for rlocus% varying alpha.
s = tf('s');
```

```
Mnm=0.3;
Mns=0.1;
a=1;
b=1;
g_dis=700;
g_reac=700;
Kp=8600;
Kf=1.16;
Ke=3500;
De=10;
Ze=Ke+s*De;
```

```
Gte=g_reac/(g_reac+s);
Gsd=g_dis/(g_dis+s);
Kvm=2*(Mns*Kp/b)^(0.5);
Kvs=2*(Mnm*Kp)^(0.5);
Cpm=Kp+Kvm*s;
Cps=Kp+Kvs*s;
Cf=Kf;
points=40;
```

```
av=linspace(1,4000,points);
```

```
for i=1:points
    a=av(i);
    U=s^2+(a*Cps+b*Cpm)/(Mnm*Mns);
    V=Mnm*(s^2+b*Cpm/(Mnm*Mns));
    W=Mnm*(s^2+a*Cps/(Mnm*Mns));
    I=Gte*Cf*(Mnm/Mns)*a+b+Gsd*Mnm;
    D=Gte*Cf*U+Gsd*Cps/Mnm;
```

```
H11=(Mnm^2*s^2*U)/D;
H12=Mnm*(Gte*Cf*b*U+Gsd*V)/(Mns*D);
H21=(Gte*Cf*a*(Mnm/Mns)*U+Gsd*W)/D;
H22=Gsd*I/(Mns*D);
```

```
T1=H21/(H11+H12*Ze);
```

```
plot(pole(T1),'x');hold;
end;
```



University of Moratuwa, Sri Lanka.
Electronic Theses & Dissertations
www.lib.mrt.ac.lk

Appendix III

```

% tuned T/F for rlocus% varying beta.
s = tf('s');

Mnm=0.3;
Mns=0.1;
a=1;
b=1;
g_dis=700;
g_reac=700;
Kp=8600;
Kf=1.16;
Ke=3500;
De=10;
Ze=Ke+s*De;

Gte=g_reac/(g_reac+s);
Gsd=g_dis/(g_dis+s);
Kvm=2*(Mns*Kp/b)^(0.5);
Kvs=2*(Mnm*Kp)^(0.5);
Cpm=Kp+Kvm*s;
Cps=Kp+Kvs*s;
Cf=Kf;
points=40;

av=linspace(1,2000,points);
for i=1:points
    b=av(i);
    U=s^2+(a*Cps+b*Cpm)/(Mnm*Mns);
    V=Mnm*(s^2+b*Cpm/(Mnm*Mns));
    W=Mnm*(s^2+a*Cps/(Mnm*Mns));
    I=Gte*Cf*(Mnm/Mns)*a+b)+Gsd*Mnm;
    D=Gte*Cf*U+Gsd*Cps/Mnm;

    H11=(Mnm^2*s^2*U)/D;
    H12=Mnm*(Gte*Cf*b*U+Gsd*V)/(Mns*D);
    H21=(Gte*Cf*a*(Mnm/Mns)*U+Gsd*W)/D;
    H22=Gsd*I/(Mns*D);

    T1=H21/(H11+H12*Ze);

plot(pole(T1),'x');hold;
end;

```



Appendix IV

```

% tuned T/F for rlocus% varying Kp
s = tf('s');

Mnm=0.3;
Mns=0.1;
a=2;
b=2;
g_dis=700;
g_reac=700;
Kp=1;
Kf=1.16;
Ke=3500;
De=10;
Ze=Ke+s*De;

points=40;
av=linspace(1,8600,points);

for i=1:points
    Kp=av(i);
    Gte=g_reac/(g_reac+s);
    Gsd=g_dis/(g_dis+s);
    Kvm=2*(Mns*Kp/b)^(0.5);
    Kvs=2*(Mnm*Kp)^(0.5);
    Cpm=Kp+Kvm*s;
    Cps=Kp+Kvs*s;
    Cf=Kf;
    U=s^2+(a*Cps+b*Cpm)/(Mnm*Mns);
    V=Mnm*(s^2+b*Cpm/(Mnm*Mns));
    W=Mnm*(s^2+a*Cps/(Mnm*Mns));
    I=Gte*Cf*((Mnm/Mns)*a+b)+Gsd*Mnm;
    D=Gte*Cf*U+Gsd*Cps/Mnm;

    H11=(Mnm^2*s^2*U)/D;
    H12=Mnm*(Gte*Cf*b*U+Gsd*V)/(Mns*D);
    H21=(Gte*Cf*a*(Mnm/Mns)*U+Gsd*W)/D;
    H22=Gsd*I/(Mns*D);

    T1=H21/(H11+H12*Ze);

plot(pole(T1),'x');hold;
end;

```



University of Moratuwa, Sri Lanka.
Electronic Theses & Dissertations
www.lib.mrt.ac.lk